Stem Cell Research 49 (2020) 102046

Contents lists available at ScienceDirect

Stem Cell Research

journal homepage: www.elsevier.com/locate/scr

Generation of pure monocultures of human microglia-like cells from induced pluripotent stem cells

Poulomi Banerjee[a,b], Evdokia Paza[a,b], Emma M. Perkins[a,b], Owen G. James[a,b], Boyd Kenkhuis[a,b,c], Amy F. Lloyd[a,b], Karen Burr[a,b], David Story[a,b], Dilmurat Yusuf[d], Xin He[b,e], Rolf Backofen[d,f], Owen Dando[b,e], Siddharthan Chandran[a,b,1], Josef Priller[a,b,g,1,*]

[a] Centre for Clinical Brain Sciences, University of Edinburgh, Edinburgh, UK
[b] UK Dementia Research Institute at University of Edinburgh, Edinburgh, UK
[c] Department of Human Genetics, Leiden University Medical Center, Leiden, The Netherlands
[d] Bioinformatics Group, Department of Computer Science, University of Freiburg, Freiburg, Germany
[e] Centre for Discovery Brain Sciences, University of Edinburgh, Edinburgh, UK
[f] Signalling Research Centres BIOSS and CIBSS, University of Freiburg, Freiburg, Germany
[g] Department of Neuropsychiatry and Laboratory of Molecular Psychiatry, Charité, Universitätsmedizin Berlin, BIH and DZNE, Berlin, Germany

ARTICLE INFO

Keywords:
Nervous system
Myeloid cells
Microglia
Transcriptome
Organoid

ABSTRACT

Microglia are resident tissue macrophages of the central nervous system (CNS) that arise from erythromyeloid progenitors during embryonic development. They play essential roles in CNS development, homeostasis and response to disease. Since microglia are difficult to procure from the human brain, several protocols have been developed to generate microglia-like cells from human induced pluripotent stem cells (hiPSCs). However, some concerns remain over the purity and quality of *in vitro* generated microglia. Here, we describe a new protocol that does not require co-culture with neural cells and yields cultures of 100% $P2Y_{12}^{+}$ 95% $TMEM119^{+}$ ramified human microglia-like cells (hiPSC-MG). In the presence of neural precursor cell-conditioned media, hiPSC-MG expressed high levels of human microglia signature genes, including *SALL1*, *CSF1R*, *P2RY12*, *TMEM119*, *TREM2*, *HEXB* and *SIGLEC11*, as revealed by whole-transcriptome analysis. Stimulation of hiPSC-MG with lipopolysaccharide resulted in downregulation of $P2Y_{12}$ expression, induction of *IL1B* mRNA expression and increase in cell capacitance. HiPSC-MG were phagocytically active and maintained their cell identity after transplantation into murine brain slices and human brain spheroids. Together, our new protocol for the generation of microglia-like cells from human iPSCs will facilitate the study of human microglial function in health and disease.

1. Introduction

Microglia are the primary immune effector cells of the central nervous system (CNS). They belong to the mesodermal lineage and arise from 'primitive' erythromyeloid progenitors in the yolk sac before the development of neuroectodermal cells such as neurons, astrocytes and oligodendrocytes (Ginhoux et al., 2010). In contrast to most peripheral tissue macrophages, microglia are not replaced by 'definitive' erythromyeloid progenitors at later stages of development (Ginhoux et al., 2010; Schulz et al., 2012; Kierdorf et al., 2013). During embryonic and postnatal life, microglia undergo a stepwise maturation programme in synchrony with the CNS until they reach the adult stage (Matcovitch-Natan et al., 2016; Masuda et al., 2019). At this point, most microglia display a ramified morphology with highly motile protrusions that continuously survey the microenvironment (Davalos et al., 2005; Nimmerjahn et al., 2005). Microglia play a crucial role in CNS development by stimulating neurogenesis, promoting myelination, controlling the numbers and fate of neural cells, and modulating neuronal wiring (Marín-Teva et al., 2004; Ueno et al., 2013; Squarzoni et al., 2014; Hagemeyer et al., 2017). In the postnatal brain, they help to maintain CNS homeostasis by phagocytosing apoptotic cells (Sierra et al., 2010), pruning synapses and shaping neural circuits (Tremblay et al., 2010; Schafer et al., 2012).

Microglia are rapidly activated in response to CNS damage. They

* Corresponding author at: Centre for Clinical Brain Sciences and UK Dementia Research Institute at University of Edinburgh, Chancellor's Building, 49 Little France Crescent, EH16 4SB, UK.
E-mail address: josef.priller@ed.ac.uk (J. Priller).
[1] Shared senior authorship.

https://doi.org/10.1016/j.scr.2020.102046
Received 4 March 2020; Received in revised form 1 October 2020; Accepted 9 October 2020
Available online 14 October 2020

retract their processes and may transform into an ameboid morphology (Davalos et al., 2005; Nimmerjahn et al., 2005). Activated microglia can secrete proinflammatory cytokines and reactive oxygen species, which may aggravate CNS damage (Prinz and Priller, 2014). Pre- and perinatal activation of microglia as a result of maternal infections or obstetric complications represents a major risk factor for neurodevelopmental disorders like schizophrenia, autism spectrum disorder, childhood epilepsy and cerebral palsy (Knuesel et al., 2014). Moreover, many genetic alterations that have been associated with late-onset neurodegenerative diseases like amyotrophic lateral sclerosis (ALS), frontotemporal dementia (FTD), Parkinson's disease (PD) and Alzheimer's disease (AD) directly affect microglial function (Prinz and Priller, 2014). As a result, the interest in understanding cell-autonomous and non-autonomous functions of microglia in neurological and psychiatric disorders has increased.

Unfortunately, studying the functions of human microglia is challenging because samples of good-quality human CNS tissue are sparse, in particular for rare diseases. The isolation of microglia from post-mortem tissue or surgery specimens may introduce technical artefacts, and the impact of confounding factors such as comorbidities, medication, distress is considerable. Moreover, microglia identity is highly dependent on environmental factors, and the characteristic signatures of microglia are rapidly lost after isolation from the brain (Gosselin et al., 2014). Attempts to generate microglia-like cells from peripheral blood monocytes or to immortalize human fetal microglia failed to replicate the phenotype of cultured primary human microglia (Melief et al., 2016).

Some of these limitations may be overcome by the use of pluripotent stem cells. Embryonic stem cells (ESCs) isolated from blastocysts and induced pluripotent stem cells (iPSCs) derived from somatic cells (Takahashi and Yamanaka, 2006) provide an unlimited supply of human stem cells that can be differentiated into any type of tissue. Despite of some concerns about epigenetic memory (Kim et al., 2010; Bar-Nur et al., 2011) and chromosomal instability (Yoshihara et al., 2017), the iPSC technology has proven to be extremely helpful in modelling human genetic disorders (Rowe and Daley, 2019). The ethical concerns associated with ESCs are avoided, and gene editing technologies like CRISPR allow for the generation of isogenic control lines that help to overcome the problems associated with variability across different lines. Human iPSCs can be differentiated into monocytes and macrophages without the use of feeder cells by adding interleukin (IL)-3 and macrophage colony stimulating factor (M-CSF, CSF-1) to drive monocytopoiesis (van Wilgenburg et al., 2013) via the formation of primitive streak and haemangioblasts (Slukvin, 2013). Human iPSC-derived macrophages (hiPSC-Mac) develop in a *MYB*-independent fashion (Buchrieser et al., 2017), and acquire a microglia-like phenotype upon co-culture with human iPSC-derived cortical neurons (Haenseler et al., 2017a). Alternative protocols to generate microglia-like cells from human iPSCs require multiple tituration steps (Muffat et al., 2016), cell sorting (Douvaras et al., 2017), or fluorescence-activated cell sorting (FACS) and co-culture with human astrocytes (Pandya et al., 2017), resulting in lower yields. Abud *et al.* (Abud et al., 2017) presented a two-step fully-defined, serum-free protocol with high yield employing transient hypoxia and FACS. Similarly, Konttinen *et al.* (Konttinen et al., 2019) used small molecules under hypoxic conditions to differentiate hiPSCs into microglia-like cells. Recently, a simplified method to generate microglia-like cells from human iPSCs based on exposure to IL-34, M-CSF and transforming growth factor beta (TGFβ)-1 was presented by McQuade *et al.* (McQuade et al., 2018).

Since microglia develop in synchrony with the developing CNS, we hypothesized that exposure of mesodermal progenitors to the secretome of neural precursor cells (NPCs) might best mimic the environmental cues that yolk sac-derived erythromyeloid progenitors receive in the embryonic human brain. In fact, yolk sac-derived A2 progenitors in the mouse give rise to cells with the typical morphology and gene expression of microglia at the same time as neurons develop, but long before astroglia or oligodendroglia are generated after embryonic day 16 (Costa et al., 2009; Kierdorf et al., 2013; Hagemeyer et al., 2016). Here, we present a novel neurodevelopmentally guided protocol for the generation of microglia-like cells from human iPSCs (hiPSC-MG) based on NPC-conditioned media, which yields pure monocultures of human microglia-like cells.

2. Materials and methods

2.1. Maintenance of human iPSCs (hiPSCs)

All stem cell work was performed with ethical approval by the University of Edinburgh, Lothian Research and Development (2014/0303), Scotland A Research Ethics Committee (14/SS/0039). Dermal fibroblasts were reprogrammed into the hiPSC cell line GS8 (female) using non-integrating episomal plasmids. Plasmids for Oct4/shP53, SOX2/Klf4 and L-Myc/Lin28 (pCXLE-hSK and pCXLE-hUL, Addgene plasmids 27077, 27078, 27080) were electroporated into dermal fibroblasts using an Amaxa Nucleofection Kit (Lonza) (Malavasi et al., 2018). For the generation of the hiPSC line 34D6 (female), a commercially available dermal fibroblast line from ATCC (ATCC® CRL-2524™) was reprogrammed using retroviral vectors encoding OCT4, SOX2, KLF4, and c-MYC as described by Park *et al.* (Park et al., 2008). Colonies were selected between days 21–25 after culturing them on matrigel. The lines were previously reported to give rise to neural precursors, cortical neurons and motor neurons in different laboratories (Livesey et al., 2016; Bilican et al., 2012; Telezhkin et al., 2018). The cell lines were confirmed to be mycoplasma-free and karyotypically normal via G-banding. Pluripotency of all lines was confirmed via PluriTest (https://pluritest.org) and further validated using the Human Pluripotent Stem Cell Functional Identification Kit (R&D Systems). The iPSCs were maintained on growth factor-reduced, feeder-free 6-well plates coated with Matrigel (Scientific Laboratory Supplies) for 1 h in a humidified incubator (5% CO_2, 37 °C). Matrigel was diluted 1:60 by adding 10 ml of cold advanced DMEM (Gibco) to 10 ml of Matrigel, followed by a 1:30 dilution with ice-cold advanced DMEM. The cells were fed with Essential 8 (E 8, Gibco) every day and passaged weekly using 0.5 mg/ml dispase (Thermo Fisher Scientific) and 1.0 mg/ml collagenase (Thermo Fisher Scientific).

2.2. Differentiation of hiPSCs into cortical neural precursor cells (NPCs)

Human iPSC-derived cortical NPCs were generated as described previously (Bilican et al., 2014). Briefly, hiPSC colonies were enzymatically lifted and induced towards a neuronal fate in chemically defined medium. For making 500 ml of chemically defined media, 0.5% BSA was dissolved in 1:1 IMDM/F12 followed by addition of 5 ml lipids (1%), 350 µl insulin (7 µg/ ml), 250 µl transferrin (15 µg/ ml), 20 µl monothioglycerol (450 µM) with 5 ml PSF (1%) (Gibco). After filtering through 0.22 µm filters, the solutions were stored at 4 °C for up to 10 – 14 days. This chemically defined media was supplemented with N-acetyl cysteine (100 ng/ml; Sigma), activin inhibitor (10 ng/ml; R&D systems) and LDN 19,318 (100 ng/ml; Stratech) for one week to induce neuronal differentiation. Subsequently, the medium was replaced by base medium (advanced DMEM/F12, 1X P/S, 1X Glutamax, 1X N2) supplemented with 2.5 ng/ml FGF2 (Peprotech) and 0.4% B27 (Gibco). After 7–10 days, the neurospheres were transferred onto plates coated with laminin (Sigma-Aldrich). Laminin was thawed slowly at 2–8 °C and reconstituted in 1X PBS to yield a final concentration of 50 µg/ml. The neural rosettes were dissociated with accutase (Sigma-Aldrich) and the cells were plated onto 6-well plates that were coated with laminin for 1 h. They were cultured in base media supplemented with 0.1% B27 and 10 ng/ml FGF2 under hypoxic conditions (3% O_2). The NPCs were passaged 1:2 with accutase once a week and fed with a total of 7 ml of the above medium twice a week. The NPC-conditioned medium used

for hiPSC-MG differentiation was collected weekly after passages 5–6, and centrifuged at 2,000 rpm before adding onto cells.

2.3. Differentiation of hiPSCs into myeloid precursors

Human iPSC-derived myeloid precursors were generated using defined conditions as previously described by Haenseler *et al.* (Haenseler et al., 2017a), and differentiated into microglia-like cells recapitulating the same developmental milestones but with small adaptations from Haenseler *et al.* (Haenseler et al., 2017a). The hiPSC colonies were enzymatically lifted for embryoid body (EB) formation using dispase/collagenase and cultured in E8 medium in a 10 cm-dish on a shaker inside a humidified incubator. The following day, 50 ng/ml BMP-4 (Peprotech), 50 ng/ml VEGF (Peprotech) and 25 ng/ml SCF (Miltenyi Biotec) were added for mesodermal lineage patterning. Media were changed daily for 4–6 days, after which the newly formed spheres were plated onto Matrigel-coated 6-well plates at a density of 20–30 spheres per well and kept in myeloid differentiation medium. Myeloid differentiation medium consisted of X-VIVO 15 (Lonza), 1x (2 mM) Glutamax (Gibco), 1X antibiotic–antimycotic (Gibco), 1X Non-Essential amino acids (Gibco), 50 μM β-mercaptoethanol (Gibco), supplemented with 25 ng/ml IL-3 (Peprotech) and a weekly increasing gradient of 50, 80, 100 ng/ml M-CSF (Peprotech). Fresh media were added every other day. After 4 weeks, the attached EBs started to form transparent spheres, which acted as “myeloid factories” producing myeloid precursors floating in the supernatant.

2.4. Differentiation of myeloid precursors into macrophages and microglia-like cells

Myeloid precursors were collected weekly from the supernatant (for up to 16 weeks) and subsequently plated and differentiated into macrophages and microglia-like cells in 6-well plates. The plates were coated with 0.01 mg/ml poly-L-lysine (Sigma-Aldrich) and 0.01% gelatin (Sigma-Aldrich). For the generation of macrophages (hiPSC-Mac), myeloid precursors were cultured in myeloid differentiation base medium supplemented with 100 ng/ml M-CSF for at least 7 days as described by van Wilgenburg *et al.* (van Wilgenburg et al., 2013). For the differentiation into microglia-like cells (hiPSC-MG), myeloid precursors were plated onto 6-well plates coated with 0.01 mg/ml poly-L-lysine and 0.01% gelatin, and cultured in medium consisting of advanced DMEM/F12 (Gibco), 1X (2 mM) Glutamax, 1X N2-supplement, 100 U/ml penicillin, 100 μg/ml streptomycin, 0.25 μg/ml amphotericin B, 50 μM β-mercaptoethanol, supplemented with 100 ng/ml IL-34 (Peprotech) and 10 ng/ml GM-CSF (Peprotech). After 7 days, microglia media were supplemented every other day with an increasing gradient (10, 20, 30, 40, 50%) of NPC-conditioned media (generated as described above). The precursors were allowed to differentiate into microglia-like cells for at least 15 days before harvesting and characterization. For comparison, we also generated microglia-like cells (pMGL) with GM-CSF and IL-34 as described by Haenseler *et al.* (Haenseler et al., 2017a).

2.5. Immunocytochemistry (ICC)

Cells grown on coverslips were fixed in 4% paraformaldehyde (PFA; Agar scientific) in phosphate-buffered saline (1X PBS) for 10 min at room temperature. After fixation, cells were washed three times with 1X PBS, permeabilised with 0.1% Triton-X100 (Thermo Fisher Scientific) in 1X PBS for 5 min and blocked with 3% BSA (Europa Bioproducts) in 1X PBS for 1hr at room temperature. Incubation with primary antibodies against TMEM119, $P2Y_{12}$, CD11b, PU.1 combined with Iba1 (see Suppl. Table 1) was performed in blocking solution at 4 °C overnight. After three washes with 1X PBS, incubation with secondary antibodies (see Suppl. Table 1) was performed in blocking solution for 1 hr at room temperature in the dark. Subsequently, cells were washed three times with 1X PBS and nuclei were counterstained with 4′,6-diamidino-2-phenylindole (DAPI; Thermo Fisher Scientific) at 1:10,000 in 1X PBS for 10 min. After three washes with 1X PBS, the coverslips were mounted onto slides. Visualization of the stainings was performed using a Zeiss LSM confocal microscope.

2.6. Scanning electron microscopy (SEM)

Cells on coverslips were washed once with 1X PBS, fixed in 4% PFA/2% glutaraldehyde in 0.1 M phosphate buffer, followed by 1 hr of post-fixation treatment in 1% osmium tetroxide. They were then dehydrated in an ascending series of ethanol (50%, 70%, 90% ethanol for 15 min followed by 3 changes in 100% ethanol for 20 min). After critical point drying, the samples were carefully mounted onto an aluminium stub for SEM and imaging in the Hitachi S4700 Scanning Electron Microscope (Cryo and Ambient).

2.7. Flow cytometry

The non-adherent myeloid precursors were collected, centrifuged and washed with 1X PBS. The differentiated macrophages and microglia-like cells were enzymatically detached from the wells with 1 ml accutase (Sigma-Aldrich) for 3 min, washed with 1X PBS and centrifuged. The cells were treated with 1% Fc block (Miltenyi Biotec) in 1X PBS for 10 min at room temperature. Allophycocyanin (APC)-conjugated antibodies against CD11b, CD45 and CD163 (see Suppl. Table 1) were added for 45 min at 4 °C. For unconjugated antibodies against TMEM119, $P2Y_{12}$ and CX3CR1 (see Suppl. Table 1), cells were fixed in 2% PFA for 15 min at room temperature followed by three washes in 1X PBS. They were then centrifuged, permeabilized with 0.1% saponin (Sigma-Aldrich) in 1X PBS and blocked in 1% Fc block for 10 min. After incubation with primary antibodies for 1 hr on ice, cells were washed twice with 1X PBS and incubated with the respective secondary antibodies (see Suppl. Table 1**)** for 45 min on ice. Samples were then washed twice with 1X PBS and transferred onto round-bottom polystyrene tubes (BD Falcon) until measurement. The stained cell samples were analysed using a FACS LSR Fortessa (4 laser) flow cytometer (BD Biosciences), and the data were processed using the FlowJo software.

2.8. Functional assays

Cells were stimulated with 100 ng/ml lipopolysaccharide (LPS; Sigma-Aldrich) for 8 hr before analysis. Live bead uptake assays were performed by incubation of cells with pHrodo-conjugated zymosan beads (Thermo Fisher Scientific) at a concentration of 0.5 mg/ml in media for 2 hr in a humidified incubator (5% CO_2, 37 °C). Time lapse images were taken on a Zeiss Axio observer inverted microscope.

2.9. Electrophysiology

Whole-cell patch clamp electrophysiological recordings were performed in an extracellular recording solution comprising (in mM): 152 NaCl, 2.8 KCl, 10 HEPES, 2 CaCl2, 10 glucose at pH 7.3, 320–330 mOsm. Recordings were made at room temperature with borosilicate glass pipettes (3–5 MΩ) containing the following (in mM): 155 K-gluconate, 2 MgCl2, 10Na-HEPES, 10Na-phosphocreatine, 2 Mg2-ATP, and 0.3 Na3-GTP at pH 7.3, 300 mOsm. Cell membrane properties were calculated from the current response to a − 10 mV, 30 ms step and the average resting membrane potential was measured from a 15 s recording. Current and voltage measurements were low-pass filtered online at 2 kHz and digitized at 10 kHz using pClamp10 software (Axon).

2.10. RNA extraction, reverse transcription and polymerase chain reaction (PCR)

Cells were harvested and RNA was extracted using RNeasy Mini Kit (Qiagen). Contaminating DNA was removed using RNase-Free DNase Set (Qiagen). The RNA was reverse transcribed using RevertAid RT Reverse Transcription Kit (Thermo Fisher Scientific) according to the manufacturer's protocol. Quantitative real-time PCR (qRT-PCR) was performed with DyNAmo ColorFlash SYBR Green Master Mix (Thermo Fisher Scientific) on a CFX96™ Real Time PCR System (BioRad). Primers were synthesized by Sigma (sequences are shown in Suppl. Table 2). The annealing temperature for all primers was 58 °C. The housekeeping genes *GAPDH* and *ACTB* were used as reference and the ct values were normalised to iPSC-derived myeloid progenitors. The mRNA expression was represented as $2^{-\Delta\Delta ct}$.

2.11. RNA sequencing (RNA-seq) and bioinformatic analysis

Total RNA was extracted with RNeasy Mini Kit (Qiagen) according to the manufacturer's instructions. RNA quality and quantity were determined using NanoDrop (Denovix, DS-11). Libraries were prepared from 2 μg of total RNA using TruSeq RNA Sample Prep Kit v2 (Illumina) with a 10-cycle enrichment step according to the manufacturer's recommendations. After pooling the final libraries in equimolar proportions, Illumina sequencing was performed on a NovaSeq 6000 platform by Edinburgh Genomics, giving 50 base paired-end reads. We employed a *Galaxy* (Afgan et al., 2018) workflow that assessed sequencing qualities using *FastQC* v0.11.5{…} (Andrews and FastQC, 2015), performed sequence alignments against the human genome reference (hg38) using *STAR* v2.6.0b (Dobin et al., 2013), and counted reads mapping to gene features using the ENSEMBL gene annotation (Zerbino et al., 2018) and *featureCounts* v1.5.3 (Liao et al., 2014). *MultiQC* v1.3 (Ewels et al., 2016) was used to generate the corresponding summary statistics of each analysis step. Prior to the principal component analysis (PCA), the per gene raw counts were first subjected to a variance-stabilizing transformation using the *DESeq2* R package (Love et al., 2014), then potential batch effect was assessed using the *RUVseq* R package (Risso et al., 2014). PCA was carried out using *DESeq2* and plotted using *ggplot2* (Wickham, 2016). Differential expression (DE) analysis was performed using *DESeq2* and the log fold changes were shrunken using the shrinkage estimator *ashr* (Stephens, 2017). Gene clusters were obtained using the partitioning around medoids (PAM) algorithm available in the *cluster* R package (Maechler et al., 2005). Functional enrichment of the resulting gene clusters was computed using the *String* website (Szklarczyk et al., 2019). Heatmaps of gene clusters and functional enrichments were generated using *ComplexHeatmap* (Gu et al., 2016).

2.12. Engraftment assays

Organotypic brain slice cultures were prepared and maintained as previously described by Lloyd *et al.* (Lloyd et al., 2019). The slices were sagitally sectioned at 300 μm and six slices were cultured per Millicell-CM mesh insert (Millipore) in 6-well culture plates. HiPSC-MG were enzymatically lifted with accutase and incubated with 10 μM CFSE (Abcam) for 15 min at 37 °C to live-label the cells. After washing in fresh media, 0.5 μl of CFSE-labelled hiPSC-MG were injected into the slices at a concentration of 5,000 cells/μl using a Hamilton syringe. The slices were incubated at 37 °C/ 5% CO_2 for 72 h, then fixed in 4% PFA (Sigma-Aldrich) for 10 min at room temperature, followed by three washes in 1X PBS. After permeabilization and blocking in 1X PBS containing 5% horse serum (Vector Laboratories) and 0.3% Triton-X 100 for 1 h, incubation with primary antibodies against Iba1 and human nuclear antigen (see Suppl. Table 1) was performed for 2 nights at 4 °C in a humid chamber. After three washes in 1X PBS, fluorophore-conjugated secondary antibodies (see Suppl. Table 1) were added in blocking solution and incubated at room temperature for 2 h. Slices were counterstained with Hoechst (Sigma-Aldrich), mounted onto slides, and coverslipped with Fluoromount-G (Cambridge Biosciences). Z-stacks of slices were acquired with an Olympus spinning disk confocal microscope and a 60X oil immersion objective with Slidebook software (Intelligent Imaging Innovations, Inc).

CNS-patterned spheroids were generated as described by Livesey *et al.* (Livesey et al., 2016). Briefly, hiPSCs were neuralised as a suspension culture using SB-431542 (20 μM; R&D systems) and LDN-193189 (0.1 μM; Stratech Scientific) in chemically defined media (CDM) containing 50% Iscove's modified Dulbecco's medium/ 50% F12 (Thermo Fisher), 5 mg/ml BSA (Europa-bioproducts) 1% chemically defined Lipid 100 (Thermo Fisher), 450 μM monothioglycerol (Sigma), 7 mg/ml insulin (Sigma) 15 mg/ml transferrin (Sigma) 1% Antibiotic-Antimycotic (Thermo Fisher) and 1 mM N-acetyl cysteine (Sigma). After 7 days, neurospheres were patterned towards a caudal fate by the addition of retinoic acid (1 μM; Sigma). On day 15, neurospheres were ventralised by transferring into N2/B27 medium (Advanced DMEM/ F12, 1% N2, 1% B27, 0.5% Glutamax, 1% Antibiotic-Antimycotic) containing the sonic hedgehog agonist, purmorphamine (1 μM; Merck). Ventral/ caudal-patterned progenitor cells were further expanded in the presence of FGF-2 (10 ng/ml; peprotech) for 7 days and then maintained in the absence of FGF-2 for an additional 2 weeks. At this stage, CNS-patterned spheroids contained neurons, astrocytes and oligodendrocyte progenitor cells (not shown). On day 35, 50,000 hiPSC-MG were added to the CNS-patterned spheroids in a total volume of 5 μl. After 3 days, spheroids were collected and fixed using 4% PFA for 2 hr at room temperature and washed three times in 1X PBS. Spheroids were then immersed in 30% sucrose overnight at 4 °C and frozen in O.C.T. mounting medium (Leica) before 25 μm sections were cut from individual spheroids using a Leica cryostat. For immunostaining, sections were washed in 1X PBS, permeabilised in 0.25% Triton-X 100 in 1X PBS for 10 min, and blocked in 10% BSA + 0.25% Triton-X 100 in 1X PBS for 2 h. Incubation with primary antibodies against Iba1 and Tmem119 (see Suppl. Table 1) was performed in blocking solution overnight at room temperature. Sections were then washed in 1X PBS and incubated with fluorophore-conjugated secondary antibodies (see Suppl. Table 1) in blocking solution for 2 hr. Sections were counterstained with DAPI, washed three times in 1X PBS and mounted using FluorSave (Merck). Z-stacks of sectioned spheroids were acquired using a Zeiss 710 confocal microscope with a 63X oil immersion objective.

2.13. Statistical analysis

Statistical comparison between the groups (hiPSC-MG, hiPSC-Mac, pMGLs) was performed using the one-way ANOVA test, followed by Tukey's multiple comparison test. Electrophysiology results were analysed using the Student's *t*-test with GraphPad Prism 6.00. Data are means and error bars represent standard deviation (SD) or standard error of the mean (SEM) as indicated. Statistical significance is represented as $p < 0.05$ (∗), $p < 0.01$ (∗∗), and $p < 0.001$ (∗∗∗).

3. Results

3.1. HiPSC-MG show characteristic microglial morphology and marker expression

We generated microglia-like cells from hiPSCs by trying to recapitulate *in vivo* developmental milestones (Fig. 1**A**). EBs from two independent iPSC lines that were obtained from healthy individuals were patterned towards the mesodermal lineage in medium containing BMP-4, VEGF and SCF, resulting in the highest gene expression of the key primitive streak marker *Brachyury* and *MIXL1* at day 3 (**Suppl.** Fig. 1). This was followed by haemangioblast specification indicated by the expression of *KDR* and *FLK1* mRNAs after day 3, and expression of *RUNX1* mRNA with a peak at day 14, confirming the activation of

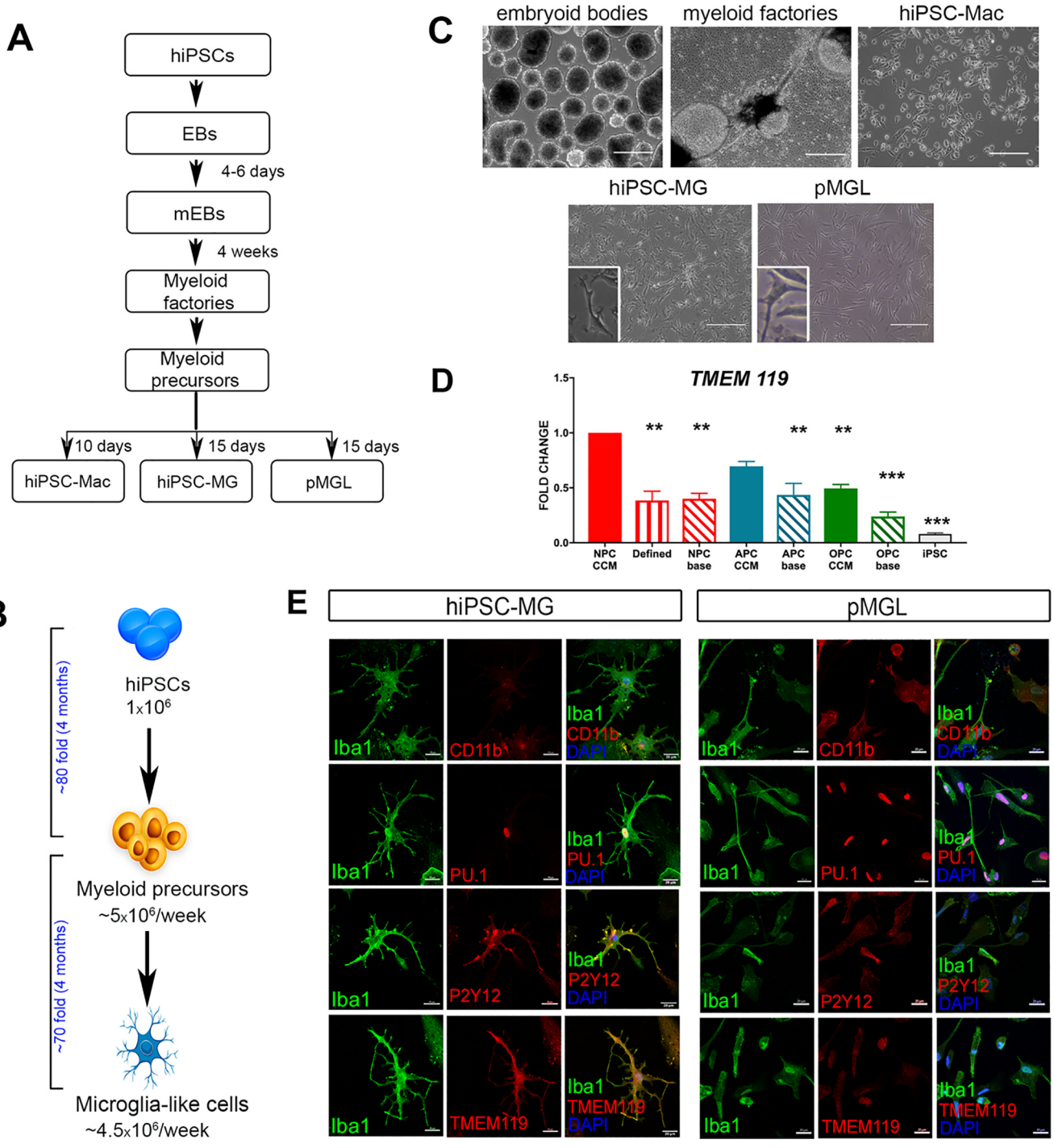

Fig. 1. Generation of hiPSC-MG (**A**) A schematic of hiPSC-MG differentiation from human induced pluripotent stem cells (hiPSCs). HiPSCs were differentiated into mesodermal embryoid bodies (mEBs), followed by patterning them towards the myeloid lineage. Myeloid precursors were produced from myeloid factories and then differentiated into macrophages (hiPSC-Mac) using M-CSF. Microglia-like cells were obtained after exposure to GM-CSF + IL-34 (pMGL), or GM-CSF + IL-34 + neural precursor cell (NPC)-conditioned medium (hiPSC-MG). (B) Schematic describing the total yield of hiPSC-MG from the initial seeding population of hiPSCs. (**C**) Representative phase contrast images of mEBs, myeloid factories, hiPSC-Mac and hiPSC-MG. Insets show hiPSC-MG and pMGL at higher magnification. Scale bars = 200 μm. (**D**) Comparison of *TMEM119* mRNA expression in hiPSC-MG obtained with NPC-conditioned media (CCM) *versus* pMGL and microglia-like cells obtained with astroglial precursor cell (APC) CCM or oligodendroglial precursor cell (OPC) CCM. "Base" indicates non-conditioned media. All values were normalised against *GAPDH* and *ACTB* mRNA expression, and the fold change was determined against hiPSC-MG obtained with NPC CCM. NPC CCM resulted in significantly higher *TMEM119* mRNA expression than all other conditions. Data is represented as ± SEM from 3 biological replicates and p value was calculated using Tukey's multiple comparisons test *versus* NPC CCM. *$p < 0.05$, **$p < 0.01$, ***$p < 0.001$. (**E**) Immunoreactivities for Iba1, CD11b, PU.1, $P2Y_{12}$ and TMEM119 in hiPSC-MG (left panel) *versus* pMGL (right panel). Nuclei were counterstained with DAPI. All experiments were performed as n = 3 in triplicate. Scale bars = 20 μm.

haematopoetic programming in a temporal manner (**Suppl.** Fig. 1). Mesodermally patterned EBs (Fig. 1A-C) were then cultured in myeloid precursor medium containing M-CSF and IL-3. After 2 weeks, the majority of EBs formed transparent cystic, yolk sac-like structures, referred to as "myeloid factories" (Fig. 1**C**). By week 4, the myeloid factories produced large, round cells with filopodia, which are considered to be myeloid precursors. The myeloid precursors expressed CD11b, CD45 and CX3CR1 (**Suppl.** Fig. 2). Myeloid factories were maintained for 4 months, and the yield of myeloid precursors above the initial seeding population of hiPSCs was around 80-fold. Myeloid precursors were differentiated into macrophages (hiPSC-Mac) in the presence of M-CSF for 10 days (Fig. 1**C**). When myeloid precursors were exposed to an increasing gradient (10–50%) of NPC-conditioned medium (irrespective of the originating hiPSC line as shown in **Suppl.** Fig. 3) plus IL-34 and GM-CSF, microglia-like cells (hiPSC-MG) developed with the typical ramified morphology of microglia (Fig. 1**C and E**) within 12–15 days. The total time taken to generate hiPSC-MG from hiPSCs was 45–50 days, and the yield of hiPSC-MG from a single hiPSC was 65–70-fold over a period of 4 months (Fig. 1**B**). Exposure to NPC-conditioned medium is believed to mimic aspects of the crosstalk between neurogenesis and microgliogenesis during normal brain development, which may explain why the procedure is more efficient in generating hiPSC-derived cells that express the *bona fide* microglia marker gene *TMEM119* than exposure to astroglial or oligodendroglial precursor cell-conditioned media (Fig. 1**D**). In contrast to microglia-like cells generated in defined medium supplemented with GM-CSF and IL-34 (pMGL) as described by Haenseler *et al.* (Haenseler et al., 2017a), the expression levels of *TMEM119* mRNA and protein were higher in hiPSC-MG (Fig. 1**D and E**). HiPSC-MG also expressed the microglia marker $P2Y_{12}$ and the myeloid markers PU.1 and CD11b as shown by immunocytochemistry (Fig. 1**E**). FACS analysis revealed a high percentage of TMEM119 (95%) and $P2Y_{12}$ (100%) expression in hiPSC-MG (Fig. 2**A and D**) when compared to hiPSC-Mac (Fig. 2**C and D**), and a lower expression of CD11b, CD45 and the haemoglobin scavenger receptor CD163 when compared to pMGL and hiPSC-Mac (Fig. 2**E-G**). Notably, hiPSC-MG, pMGLs and hiPSC-Mac were positive for CX3CR1 expression (Fig. 2**A–D**). In sum, hiPSC-MG show characteristic phenotypic features of human microglia.

3.2. The transcriptomic profile of hiPSC-MG resembles human microglia

We next performed a comparative RNA-seq analysis of hiPSCs, hiPSC-Mac, pMGL and hiPSC-MG generated from the same starting hiPSC lines (Fig. 3). Principal component analysis (PCA) of gene expression revealed a clear separation of hiPSCs from the progeny of macrophages and microglia-like cells in the first principal component (PC1: 83%), and PC2 (12%) showed the separation of hiPSC-Mac from pMGL and hiPSC-MG, underscoring their different developmental trajectories (Fig. 3**A**). After normalization to hiPSCs, 8 clusters of differentially expressed (DE) genes were detected between hiPSC-Mac, pMGL and hiPSC-MG (**Suppl.** Fig. 4**A**). These clusters were analysed for functional enrichment of gene ontology (GO) terms in the "biological process" domain, and the top 50 genes driving PC1 and/or PC2 were annotated (**Suppl.** Fig. 4**B**). The genes driving PC1, which separates hiPSCs from the myeloid lineage-patterned cell types (pMGL, hiPSC-MG and hiPSC-Mac), were mainly located in gene cluster 1 (genes up-regulated *versus* hiPSCs) and cluster 8 (genes down-regulated *versus* hiPSCs). Cluster 1 genes were enriched in GO terms related to response to stimulus, defense response and cell communication. The genes driving PC2, which partitions the populations of macrophages and microglia-like cells, were spread across the clusters but the majority appeared in gene cluster 6. Enriched GO terms unique to cluster 6 were related to extracellular matrix organisation, cell adhesion, blood vessel enrichment and locomotion. Next, we wanted to understand the behaviour of core microglia signature genes in hiPSC-MG. We selected the top 100 most up-regulated genes in human microglia from post-mortem brain tissue (right parietal cortex) (Galatro et al., 2017) that were also expressed in microglia derived from fresh human brain biopsies (Masuda et al., 2019) in order to obtain a human-specific gene expression signature of microglia. Then, we derived the expression of this set of 100 human core microglia signature genes across hiPSCs, hiPSC-Mac, pMGL and hiPSC-MG (Fig. 3**B**). Among the genes up-regulated in hiPSC-MG and pMGL compared to hiPSC-Mac were genes encoding for CSF-1 receptor (*CSF1R*), immune-responsive receptors like Siglecs, lectin receptors, chemokine receptors, pattern recognition receptors like Toll-like receptor *(TLR)-1/5* and *CLECL1*, as well as transcription factors like *CIITA* (regulator for major histocompatibility complex class II), *TAL1* and *MNDA* (target for interferons) (**Suppl.** Fig. 4A and Fig. 3**B**).

In order to further investigate the differential expression of selected genes enriched in myeloid cells and microglia, we validated our RNA-seq results with qRT-PCR (Fig. 4). HiPSC-MG expressed higher levels of *CX3CR1* mRNA and lower levels of *ITGAM* mRNA than pMGL and hiPSC-Mac. Most notably, hiPSC-MG, but not hiPSC-Mac or pMGL, expressed *SALL1* mRNA, a transcriptional regulator defining microglia identity and function. HiPSC-MG also expressed higher levels of the microglia-enriched genes *TMEM119* and *HEXB* and the human-specific microglia gene *SIGLEC11*. In addition, hiPSC-MG expressed higher levels of *CSF1R* mRNA than pMGL and hiPSC-Mac, confirming our RNA-seq results. The phagocytosis-related genes *MERTK, GPR34* and *TREM2* were most highly expressed in hiPSC-MG compared to pMGL and hiPSC-Mac. Finally, expression of the homeostatic microglia gene *P2RY12* was enriched in hiPSC-MG and pMGL compared to hiPSC-Mac.

3.3. HiPSC-MG are functionally active

Given that the spine-bearing surface differentiates adult microglia from other tissue macrophages, we performed SEM on hiPSC-derived macrophages and microglia-like cells. Whereas hiPSC-Mac had an ameboid morphology and a ruffled surface, hiPSC-MG extended processes that were covered with numerous spines (Fig. 5**A**). It is through these processes that hiPSC-MG took up pH-sensitive zymosan beads *in vitro* (**Suppl. Movie 1**), indicating phagocytic activity. When stimulated with the bacterial antigen LPS for 8 h, hiPSC-MG became morphologically activated (Fig. 5**B**). LPS treatment down-regulated the expression of the homeostatic microglia gene *P2RY12* (Fig. 5**C**), which was corroborated at the protein level by flow cytometry (Fig. 5**D**). In addition, LPS-stimulated hiPSC-MG up-regulated the expression of the proinflammatory gene *IL1B*, as observed for microglia *in vivo*. The electrophysiological properties of microglia vary according to their activation state and therefore, using the patch clamp technique, we detected a resting membrane potential of around − 30 to − 40 mV in hiPSC-MG, which decreased in response to LPS (Fig. 5**F**). Whole cell capacitance increased and input resistance decreased in hiPSC-MG after LPS treatment (Fig. 5**G and H**).

3.4. Engraftment of hiPSC-MG in mouse brain slices and hiPSC-derived CNS spheroids

In order to test the behaviour of hiPSC-MG in a 3D CNS environment, we decided to transplant them into mouse and human CNS tissue. To this end, we first confirmed that the enzymatic detachment of hiPSC-MG from the culture plates using accutase did not change their differentiation state by showing that hiPSC-MG continued to express the microglia markers TMEM119 and $P2Y_{12}$, and low levels of the myeloid marker CD11b at 48 h after replating (**Suppl.** Fig. 5). Next, we transplanted CFSE-labelled hiPSC-MG (**Suppl.** Fig. 6) into organotypic mouse brain slices. After 2–3 days, we detected CFSE -labelled cells that expressed human nuclear antigen (HNA) and the microglia/macrophage marker Iba1, surrounded by a strong response of endogenous murine microglia ($CFSE^{-}Iba1^{+}$) to the xenotransplant (Fig. 6**A-D**). Three days after transplantation into human iPSC-derived CNS-

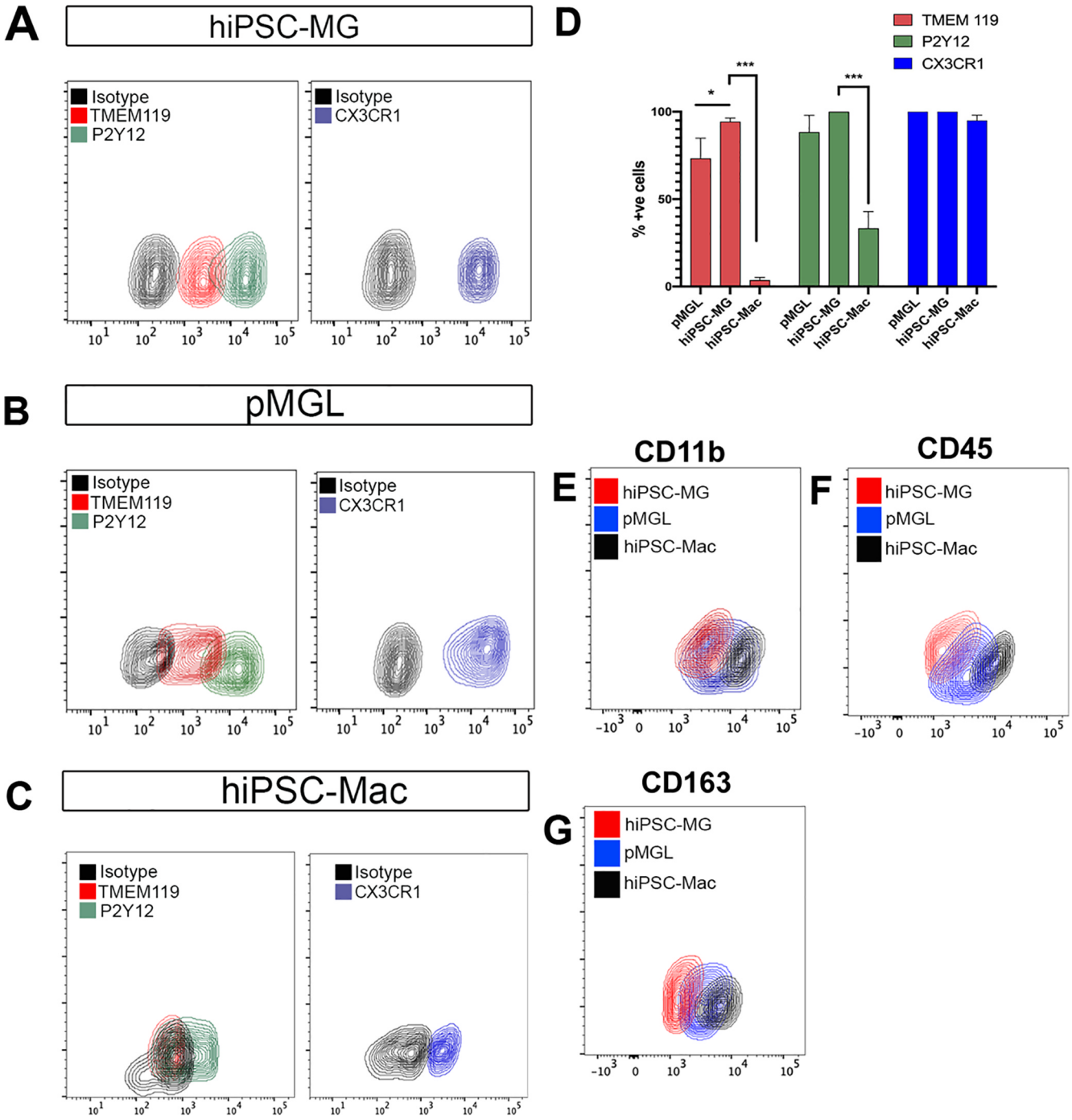

Fig. 2. Characterisation of hiPSC-MG by FACS (**A**) Representative flow cytometric expression of TMEM119, $P2Y_{12}$ (left panel) and CX3CR1 (right panel) *versus* isotype controls in hiPSC-MG. (**B**) Representative flow cytometric expression of TMEM119, $P2Y_{12}$ (left panel) and CX3CR1 (right panel) *versus* isotype controls in pMGL. (**C**) Representative flow cytometric expression of TMEM119, $P2Y_{12}$ (left panel) and CX3CR1 (right panel) *versus* isotype controls in hiPSC-Mac. (**C**) Quantification of the percentage of $TMEM119^+$, $P2Y_{12}{}^+$ and $CX3CR1^+$ pMGL, hiPSC-MG and hiPSC-Mac. Only live cells were analysed. Data are means + SEM from 3 biological replicates, p value was calculated by 2-way ANOVA using Sidak's multiple comparison test *p < 0.05, **p < 0.01, ***p < 0.001 (**E-G**) Differential flow cytometric expression of CD11b (**D**), CD45 (**E**) and CD163 (**F**) in hiPSC-MG *versus* pMGL *versus* hiPSC-Mac.

patterned spheroids, which are devoid of any mesodermal cells (data not shown), hiPSC-MG acquired a ramified morphology (**Suppl. Movie 2**), and expressed Iba1 and TMEM119 (Fig. 6**E-H**). These results demonstrate successful short-term engraftment of hiPSC-MG in mouse and human CNS tissue in the absence of immunosuppressive treatment.

4. Discussion

Here, we describe a novel protocol for the generation of human microglia-like cells from induced pluripotent stem cells (hiPSC-MG) which mimics key neurodevelopmental signals by exposure to the secretome of neural precursor cells. The method is simple, reproducible, and yields high numbers of human microglia-like cells without the need for further purification. The hiPSC-MG express *bona fide* markers of human microglia and can be directly used to study cell-autonomous and non-autonomous functions of microglia in CNS disorders.

The first study describing the generation of microglia-like cells from hiPSCs observed a significant reduction in size for Rett syndrome

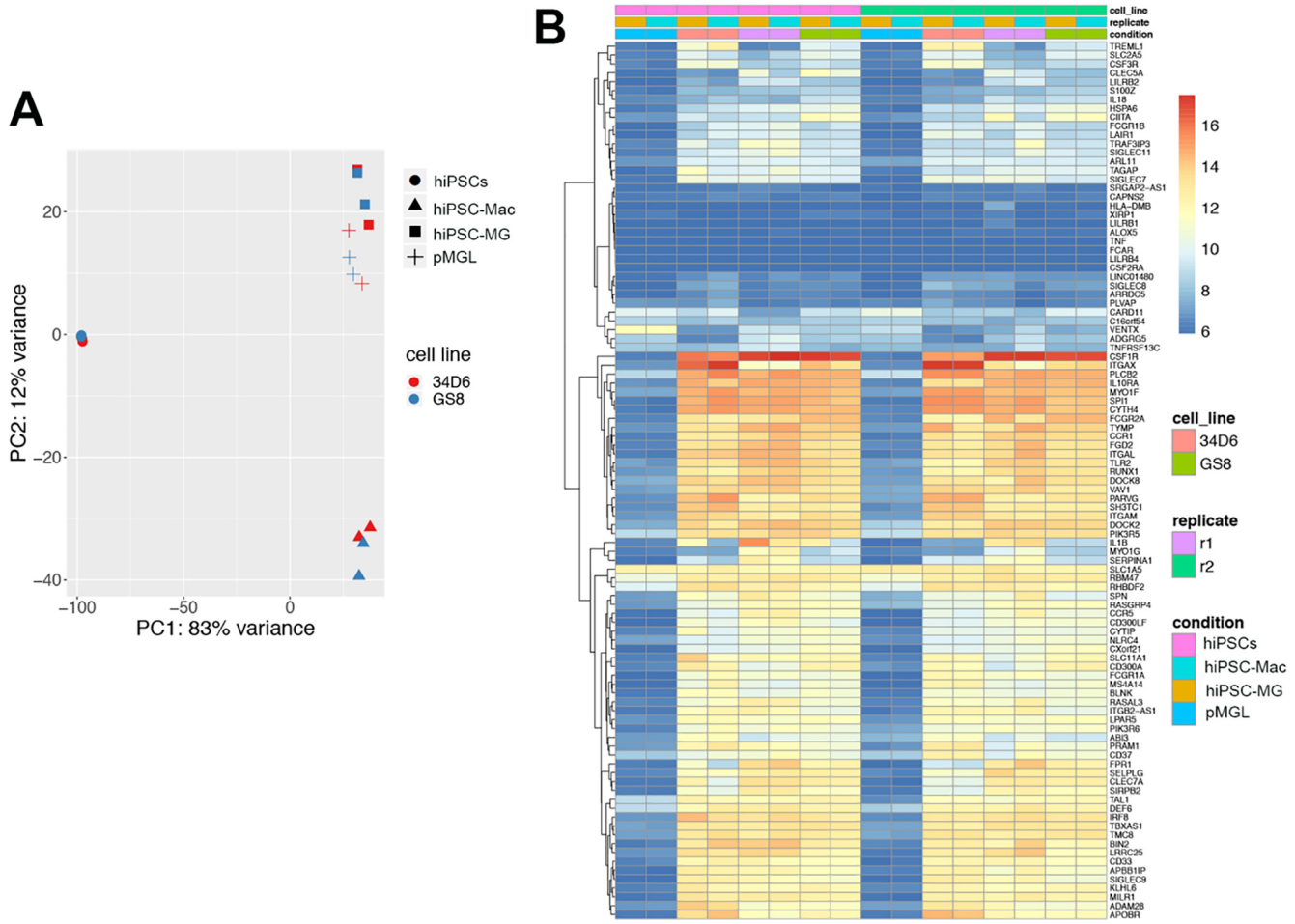

Fig. 3. Transcriptomic analysis of hiPSC-MG, pMGL and hiPSC-Mac (**A**) PCA plot of RNA-seq results for hiPSCs, hiPSC-Mac, hiPSC-MG and pMGL across 2 cell lines 34D6 and GS8. (**B**) Heatmap showing the expression of 100 human core microglia genes in hiPSCs, hiPSC-Mac, hiPSC-MG and pMGL. Blue represents lower and red represents higher gene expression.

microglia-like cells compared to isogenic controls (Muffat et al., 2016). When monocytes from patients with schizophrenia were recently differentiated into microglia-like cells by exposure to IL-34 and GM-SCF, increased engulfment of synapses from hiPSC-derived neurons was observed compared to cells from healthy controls (Sellgren et al., 2019). The pMGL generated by Haenseler *et al.* (Haenseler et al., 2017a) expressed genes whose variants have been associated with increased risk for AD, PD, ALS and FTD, including *TREM2*, *APOE*, *CD33*, *PARK15, PINK1, SNCA, C9orf72, TDP43,* and *SOD1*. Microglia-like cells derived from hiPSCs harbouring homozygous *APOE4* alleles exhibited shorter processes, reduced β-amyloid uptake, and increased expression of immune response genes compared to *APOE3* microglia-like cells (Lin et al., 2018). Moreover, hiPSC-derived macrophages from PD patients with *SCNA* triplication displayed increased intracellular α-synuclein accumulation and reduced phagocytic activity compared to cells from healthy controls (Haenseler et al., 2017b). Recently, hiPSC-derived microglia-like cells from patients with Nasu-Hakola disease caused by *TREM2* mutations exhibited a specific impairment in the phagocytosis of apoptotic bodies but not zymosan beads compared to cells from healthy controls (Garcia-Reitboeck et al., 2018). Furthermore, there is emerging evidence on the role of *TREM2* mediating lipid metabolism (Nugent et al., 2020) and glycolytic switch (Piers et al., 2020) employing human iPSC-derived microglia. These results underscore the potential of pluripotent stem cell models for studying microglia in CNS disorders.

Our new protocol for generating hiPSC-MG is developmentally guided, and the pluripotent cells are initially directed to form mesodermal cells and haemogenic endothelium by activating BMP signalling (Durand et al., 2007) (Goldman et al., 2009) and VEGF signalling (Leung et al., 2013). These haemato-endothelial clusters are then specified for myelopoesis by enhancing retinoic acid (RA) receptor activity via stimulation with IL-3 and SCF to generate myeloid progenitors (Johnson et al., 2002), which are finally cultured in the presence of IL-34 and NPC-conditioned media to generate hiPSC-MG. We believe that hiPSC-MG closely resemble human microglia due to the complex signals that they receive from NPC-conditioned medium. Notably, they express *SALL1*, which controls the transcriptional signature of microglia in rodents (Buttgereit et al., 2016). To our knowledge, *SALL1* mRNA expression has not previously been described in microglia-like cells derived from human iPSCs (Abud et al., 2017; Douvaras et al., 2017; Haenseler et al., 2017a; McQuade et al., 2018; Pandya et al., 2017). The hiPSC-MG generated by our protocol also express high levels of the homeostatic microglia markers, $P2Y_{12}$ (Butovsky et al., 2014), *TMEM119* (Bennett et al., 2016) and *HEX B* (Masuda et al., 2019). In many other protocols, the expression of TMEM119 is very low or requires induction by co-culture with neurons or transplantation into cerebral organoids (Haenseler et al., 2017a; Douvaras et al., 2017; Abud et al., 2017). Moreover, the hiPSC-MG generated by our protocol express high levels of the human-specific microglia gene *SIGLEC11* (Hayakawa et al., 2005), and the phagocytosis-related genes *MERTK, GPR34,* and *TREM2*. Notably, TREM2 has recently been shown to be most highly expressed by human microglia using single-cell mass cytometry (Böttcher et al., 2019). The expression profile of $CD11b^{+}CD45^{lo}CD163^{lo}$ on hiPSC-MG is also characteristic of human

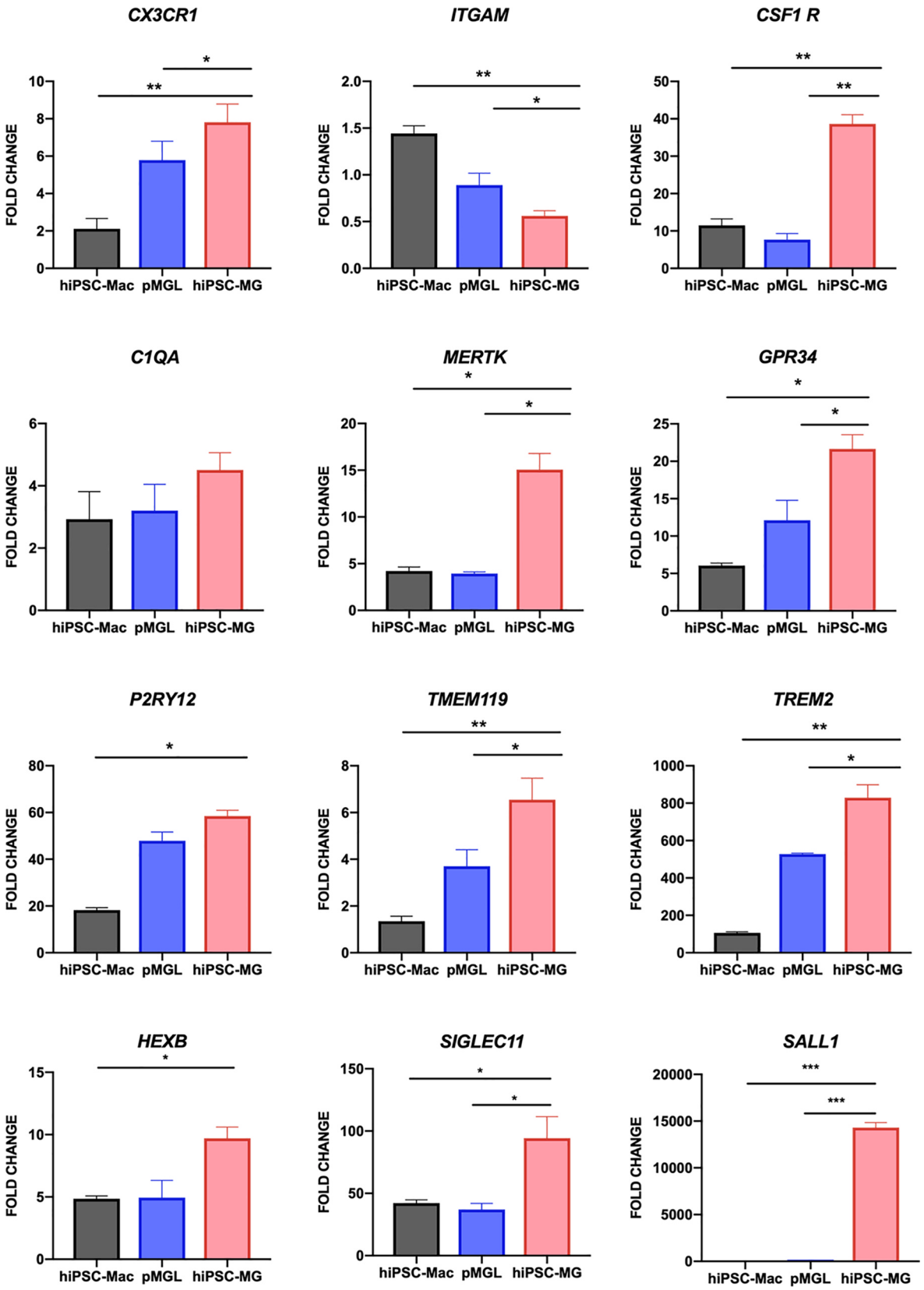

Fig. 4. qRT-PCR validation of microglia signature gene expression in hiPSC-MG, pMGL and hiPSC-Mac Expression of microglia-enriched genes was determined by qRT-PCR in hiPSC-Mac, pMGL and hiPSC-MG. Fold change was calculated by the ΔΔCT method with *GAPDH* and *ACTB* as housekeeping genes and the data was normalised to myeloid precursors (n = 3 in triplicate). Data are means + SD and statistical analysis was performed by Tukey's multiple comparison test (*p < 0.05, **p < 0.01***p < 0.001).

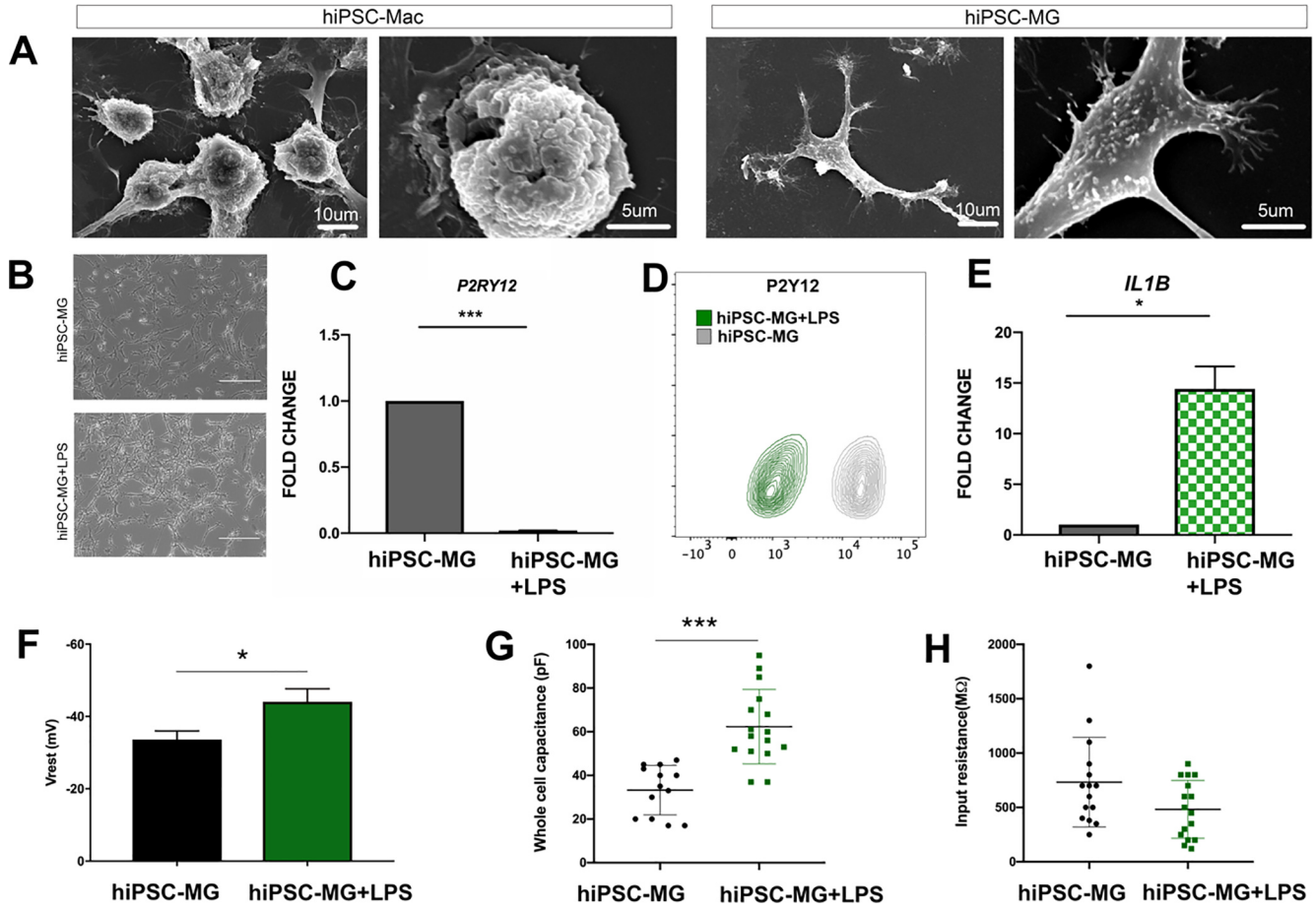

Fig. 5. Functional analysis of hiPSC-MG (A) Scanning electron micrographs of hiPSC-Mac (left panel) and hiPSC-MG (right panel) showing the characteristic "spiny" membrane ultrastructure of microglia in hiPSC-MG as opposed to membrane ruffles found on hiPSC-Mac. Scale bars = 10 μm or 5 μm as indicated. (**B**) Representative phase contrast images of hiPSC-MG before (top panel) and after (bottom panel) treatment with 100 ng/ml LPS for 8 hr. Scale bars = 200 μm. (**C**) qRT-PCR of *P2RY12* mRNA expression in hiPSC-MG before and after LPS treatment. Note the massive down-regulation of *P2RY12* mRNA expression in hiPSC-MG by LPS (***p < 0.001, n = 3 in triplicate). (**D**) Representative FACS analysis showing the down-regulation of $P2Y_{12}$ expression in hiPSC-MG after LPS treatment (n = 3 in triplicate). (**E**) qRT-PCR reveals induction of *IL1B* mRNA expression in hiPSC-MG following LPS treatment. Data are means + SD (*p < 0.05; n = 3 in triplicate). (**F**) - (**H**) Changes in resting membrane potential (**F**), whole cell capacitance (**G**) and input resistance (**H**) of hiPSC-MG after 8 hr of LPS treatment (n = 3 total number of cells analysed = 13). Statistical analysis was performed using unpaired *t* test (*p < 0.05, **p < 0.01***p < 0.001). All experiments were performed as n = 3 in triplicate.

microglia (Melief et al., 2016; Dick et al., 1997). One of the important functions of microglia is to sense changes in the microenvironment of the CNS (Hickman and El Khoury, 2019). Along these lines, our transcriptomic data revealed that hiPSC-MG express clusters of genes responsible for chemotaxis and vesicle-mediated transport like *CCR5, CX3CR1,* cysteinyl leukotriene receptors *(CYSLTR1)* and C-type lectin domain *CLEC7A*. Finally, the hiPSC-MG generated by our protocol express very high levels of *CSF1R* mRNA, which is required for the development and maintenance of human microglia. In fact, the brains of individuals with homozygous *CSF1R* mutations completely lack microglia (Guo et al., 2019; Oosterhof et al., 2019).

During recent years, a number of techniques have been developed that make use of hiPSC-derived microglia to better understand microglia biology (Hasselmann and Blurton-Jones, 2020). In an elegant set of experiments, Abud *et al.* (Abud et al., 2017) have shown that hiPSC-derived microglia engraft in hiPSC 3D cerebral organoids and in the brains of immunodeficient mice. Additionally, recent studies highlighted benefits of neonatal transplantation of hiPSC-derived microglia into mouse brains (Svoboda et al., 2019). Hasselmann *et al.* detected important transcriptional changes in the signature of hiPSC-derived microglia in response to Aβ plaques after transplantation into AD transgenic mice (Hasselmann et al., 2019). Along these lines, the hiPSC-MG generated by our protocol also engraft short-term in mouse brain slices and in hiPSC-derived CNS spheroids in the absence of immunosuppression. They show a ramified morphology and spine-bearing surface *in vitro*, which distinguishes microglia from other types of tissue macrophages (Giulian et al., 1995). The hiPSC-MG also show characteristic microglia responses to LPS stimulation, including morphological activation, down-regulation of homeostatic $P2Y_{12}$ expression (De Simone et al., 2010), transcription of proinflammatory cytokines like *IL1B* (Holguin et al., 2007), and enhanced membrane capacitance as described for rodent microglia in response to LPS (Visentin et al., 1995; Beck et al., 2008). They phagocytose zymosan particles, as described previously for other types of microglia-like cells derived from hiPSCs (Garcia-Reitboeck et al., 2018; Haenseler et al., 2017a; McQuade et al., 2018).

5. Conclusions

In sum, the hiPSC-MG generated by our protocol not only express the human core microglia signature genes, but they are also functionally active human microglia-like cells that can be tested for the effects of disease-causing mutations, interactions with other glial cells and neurons, and used as a drug screening platform. This novel protocol stands out by mimicking key neurodevelopmental signals that microglia progenitors receive during early embryonic development. The high

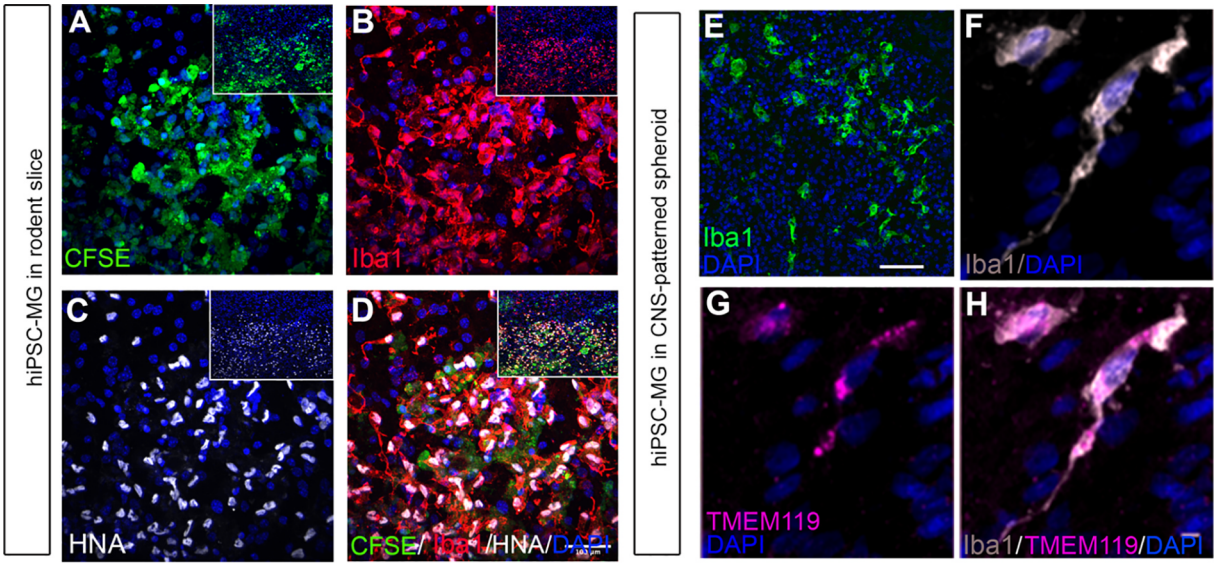

Fig. 6. Engraftment of hiPSC-MG in rodent slices and CNS-patterned spheroids (**A**) - (**D**) Representative images showing engraftment of CFSE-labelled (**A**) hiPSC-MG in mouse brain slices (n = 6) at 2 days after transplantation. HiPSC-MG co-expressed Iba1 (**B**) and human nuclear antigen (**C**). Nuclei were counterstained with DAPI (**D**). Insets in (**A**)-(**D**) show lower magnification images to reveal the extent of hiPSC-MG engraftment in the rodent slices. Scale bars = 100 μm. (**E**) - (**H**) Representative images showing engraftment of Iba1-immunoreative hiPSC-MG (**E**) in human CNS-patterned spheroids (n = 5) at 3 days after transplantation. HiPSC-MG co-expressed Iba1 (**F**) and TMEM119 (**G**) as shown in the overlay (**H**). Nuclei were counterstained with DAPI. Scale bar = 10 μm.

yield and purity of hiPSC-MG without biases introduced by cell enrichment and sorting (Kang et al., 2018; Haimon et al., 2018) represents a valuable addition to microglia developing innately within cerebral organoids (Ormel et al., 2018) for studying cell-autonomous and non-autonomous functions of microglia in neurological and psychiatric disorders.

Declaration of Competing Interest

The authors declare that they have no known competing financial interests or personal relationships that could have appeared to influence the work reported in this paper.

Acknowledgment

This work was supported by grants from the UK DRI to S.C. and J.P. (Momentum Award), MRC DPUK and Stem cell partnership, MS Society to S.C., DFG SFB/TRR167 B07 to J.P. and Z01 to Y.D. and R.B.

Appendix A. Supplementary data

Supplementary data to this article can be found online at https://doi.org/10.1016/j.scr.2020.102046.

References

Abud, E.M., Ramirez, R.N., Martinez, E.S., Healy, L.M., Nguyen, C.H.H., Newman, S.A., Yeromin, A.V., Scarfone, V.M., Marsh, S.E., Fimbres, C., Caraway, C.A., Fote, G.M., Madany, A.M., Agrawal, A., Kayed, R., Gylys, K.H., Cahalan, M.D., Cummings, B.J., Antel, J.P., Mortazavi, A., Carson, M.J., Poon, W.W., Blurton-Jones, M., 2017. iPSC-derived human microglia-like cells to study neurological diseases. Neuron 94, 278–293.e9. https://doi.org/10.1016/j.neuron.2017.03.042.

Afgan, E., Baker, D., Batut, B., van den Beek, M., Bouvier, D., Cech, M., Chilton, J., Clements, D., Coraor, N., Grüning, B.A., Guerler, A., Hillman-Jackson, J., Hiltemann, S., Jalili, V., Rasche, H., Soranzo, N., Goecks, J., Taylor, J., Nekrutenko, A., Blankenberg, D., 2018. The Galaxy platform for accessible, reproducible and collaborative biomedical analyses: 2018 update. Nucleic Acids Res. 46, W537–W544. https://doi.org/10.1093/nar/gky379.

Andrews, S., FastQC, A., 2015. A quality control tool for high throughput sequence data. 2010. Google Scholar.

Bar-Nur, O., Russ, H.A., Efrat, S., Benvenisty, N., 2011. Epigenetic memory and preferential lineage-specific differentiation in induced pluripotent stem cells derived from human pancreatic islet beta cells. Cell Stem Cell 9, 17–23. https://doi.org/10.1016/j.stem.2011.06.007.

Beck, A., Penner, R., Fleig, A., 2008. Lipopolysaccharide-induced down-regulation of Ca2+ release-activated Ca2+ currents (I CRAC) but not Ca2+-activated TRPM4-like currents (I CAN) in cultured mouse microglial cells. J. Physiol. (Lond.) 586, 427–439. https://doi.org/10.1113/jphysiol.2007.145151.

Bennett, M.L., Bennett, F.C., Liddelow, S.A., Ajami, B., Zamanian, J.L., Fernhoff, N.B., Mulinyawe, S.B., Bohlen, C.J., Adil, A., Tucker, A., Weissman, I.L., Chang, E.F., Li, G., Grant, G.A., Hayden Gephart, M.G., Barres, B.A., 2016. New tools for studying microglia in the mouse and human CNS. Proc. Natl. Acad. Sci. USA 113, E1738–E1746. https://doi.org/10.1073/pnas.1525528113.

Bilican, B., Livesey, M.R., Haghi, G., Qiu, J., Burr, K., Siller, R., Hardingham, G.E., Wyllie, D.J.A., Chandran, S., 2014. Physiological normoxia and absence of EGF is required for the long-term propagation of anterior neural precursors from human pluripotent cells. PLoS One 9, e85932. https://doi.org/10.1371/journal.pone.0085932.

Bilican, B., Serio, A., Barmada, S.J., Nishimura, A.L., Sullivan, G.J., Carrasco, M., Phatnani, H.P., Puddifoot, C.A., Story, D., Fletcher, J., Park, I.-H., Friedman, B.A., Daley, G.Q., Wyllie, D.J.A., Hardingham, G.E., Wilmut, I., Finkbeiner, S., Maniatis, T., Shaw, C.E., Chandran, S., 2012. Mutant induced pluripotent stem cell lines recapitulate aspects of TDP-43 proteinopathies and reveal cell-specific vulnerability. Proc. Natl. Acad. Sci. USA 109, 5803–5808. https://doi.org/10.1073/pnas.1202922109.

Böttcher, C., Schlickeiser, S., Sneeboer, M.A.M., Kunkel, D., Knop, A., Paza, E., Fidzinski, P., Kraus, L., Snijders, G.J.L., Kahn, R.S., Schulz, A.R., Mei, H.E., NBB-Psy, Hol, E.M., Siegmund, B., Glauben, R., Spruth, E.J., de Witte, L.D., Priller, J., 2019. Human microglia regional heterogeneity and phenotypes determined by multiplexed single-cell mass cytometry. Nat. Neurosci. 22, 78–90. https://doi.org/10.1038/s41593-018-0290-2.

Buchrieser, J., James, W., Moore, M.D., 2017. Human Induced Pluripotent Stem Cell-Derived Macrophages Share Ontogeny with MYB-Independent Tissue-Resident Macrophages. Stem Cell Rep. 8, 334–345. https://doi.org/10.1016/j.stemcr.2016.12.020.

Butovsky, O., Jedrychowski, M.P., Moore, C.S., Cialic, R., Lanser, A.J., Gabriely, G., Koeglsperger, T., Dake, B., Wu, P.M., Doykan, C.E., Fanek, Z., Liu, L., Chen, Z., Rothstein, J.D., Ransohoff, R.M., Gygi, S.P., Antel, J.P., Weiner, H.L., 2014. Identification of a unique TGF-β-dependent molecular and functional signature in microglia. Nat. Neurosci. 17, 131–143. https://doi.org/10.1038/nn.3599.

Buttgereit, A., Lelios, I., Yu, X., Vrohlings, M., Krakoski, N.R., Gautier, E.L., Nishinakamura, R., Becher, B., Greter, M., 2016. Sall1 is a transcriptional regulator defining microglia identity and function. Nat. Immunol. 17, 1397–1406. https://doi.org/10.1038/ni.3585.

Costa, M.R., Bucholz, O., Schroeder, T., Götz, M., 2009. Late origin of glia-restricted progenitors in the developing mouse cerebral cortex. Cereb. Cortex 19 (Suppl 1), i135–i143. https://doi.org/10.1093/cercor/bhp046.

Davalos, D., Grutzendler, J., Yang, G., Kim, J.V., Zuo, Y., Jung, S., Littman, D.R., Dustin, M.L., Gan, W.-B., 2005. ATP mediates rapid microglial response to local brain injury in vivo. Nat. Neurosci. 8, 752–758. https://doi.org/10.1038/nn1472.

De Simone, R., Niturad, C.E., De Nuccio, C., Ajmone-Cat, M.A., Visentin, S., Minghetti, L., 2010. TGF-β and LPS modulate ADP-induced migration of microglial cells through P2Y1 and P2Y12 receptor expression. J. Neurochem. 115, 450–459. https://doi.org/10.1111/j.1471-4159.2010.06937.x.

Dick, A.D., Pell, M., Brew, B.J., Foulcher, E., Sedgwick, J.D., 1997. Direct ex vivo flow

cytometric analysis of human microglial cell CD4 expression: examination of central nervous system biopsy specimens from HIV-seropositive patients and patients with other neurological disease. AIDS 11, 1699–1708. https://doi.org/10.1097/00002030-199714000-00006.

Dobin, A., Davis, C.A., Schlesinger, F., Drenkow, J., Zaleski, C., Jha, S., Batut, P., Chaisson, M., Gingeras, T.R., 2013. STAR: ultrafast universal RNA-seq aligner. Bioinformatics 29, 15–21. https://doi.org/10.1093/bioinformatics/bts635.

Douvaras, P., Sun, B., Wang, M., Kruglikov, I., Lallos, G., Zimmer, M., Terrenoire, C., Zhang, B., Gandy, S., Schadt, E., Freytes, D.O., Noggle, S., Fossati, V., 2017. Directed differentiation of human pluripotent stem cells to microglia. Stem Cell Rep. 8, 1516–1524. https://doi.org/10.1016/j.stemcr.2017.04.023.

Durand, C., Robin, C., Bollerot, K., Baron, M.H., Ottersbach, K., Dzierzak, E., 2007. Embryonic stromal clones reveal developmental regulators of definitive hematopoietic stem cells. Proc. Natl. Acad. Sci. USA 104, 20838–20843. https://doi.org/10.1073/pnas.0706923105.

Ewels, P., Magnusson, M., Lundin, S., Käller, M., 2016. MultiQC: summarize analysis results for multiple tools and samples in a single report. Bioinformatics 32, 3047–3048. https://doi.org/10.1093/bioinformatics/btw354.

Galatro, T.F., Holtman, I.R., Lerario, A.M., Vainchtein, I.D., Brouwer, N., Sola, P.R., Veras, M.M., Pereira, T.F., Leite, R.E.P., Möller, T., Wes, P.D., Sogayar, M.C., Laman, J.D., den Dunnen, W., Pasqualucci, C.A., Oba-Shinjo, S.M., Boddeke, E.W.G.M., Marie, S.K.N., Eggen, B.J.L., 2017. Transcriptomic analysis of purified human cortical microglia reveals age-associated changes. Nat. Neurosci. 20, 1162–1171. https://doi.org/10.1038/nn.4597.

Garcia-Reitboeck, P., Phillips, A., Piers, T.M., Villegas-Llerena, C., Butler, M., Mallach, A., Rodrigues, C., Arber, C.E., Heslegrave, A., Zetterberg, H., Neumann, H., Neame, S., Houlden, H., Hardy, J., Pocock, J.M., 2018. Human Induced Pluripotent Stem Cell-Derived Microglia-Like Cells Harboring TREM2 Missense Mutations Show Specific Deficits in Phagocytosis. Cell Rep. 24, 2300–2311. https://doi.org/10.1016/j.celrep.2018.07.094.

Ginhoux, F., Greter, M., Leboeuf, M., Nandi, S., See, P., Gokhan, S., Mehler, M.F., Conway, S.J., Ng, L.G., Stanley, E.R., Samokhvalov, I.M., Merad, M., 2010. Fate mapping analysis reveals that adult microglia derive from primitive macrophages. Science 330, 841–845. https://doi.org/10.1126/science.1194637.

Giulian, D., Li, J., Bartel, S., Broker, J., Li, X., Kirkpatrick, J.B., 1995. Cell surface morphology identifies microglia as a distinct class of mononuclear phagocyte. J. Neurosci. 15, 7712–7726.

Goldman, D.C., Bailey, A.S., Pfaffle, D.L., Al Masri, A., Christian, J.L., Fleming, W.H., 2009. BMP4 regulates the hematopoietic stem cell niche. Blood 114, 4393–4401. https://doi.org/10.1182/blood-2009-02-206433.

Gosselin, D., Link, V.M., Romanoski, C.E., Fonseca, G.J., Eichenfield, D.Z., Spann, N.J., Stender, J.D., Chun, H.B., Garner, H., Geissmann, F., Glass, C.K., 2014. Environment drives selection and function of enhancers controlling tissue-specific macrophage identities. Cell 159, 1327–1340. https://doi.org/10.1016/j.cell.2014.11.023.

Gu, Z., Eils, R., Schlesner, M., 2016. Complex heatmaps reveal patterns and correlations in multidimensional genomic data. Bioinformatics 32, 2847–2849. https://doi.org/10.1093/bioinformatics/btw313.

Guo, L., Bertola, D.R., Takanohashi, A., Saito, A., Segawa, Y., Yokota, T., Ishibashi, S., Nishida, Y., Yamamoto, G.L., da S Franco, J.F., Honjo, R.S., Kim, C.A., Musso, C.M., Timmons, M., Pizzino, A., Taft, R.J., Lajoie, B., Knight, M.A., Fischbeck, K.H., Singleton, A.B., Ferreira, C.R., Wang, Z., Yan, L., Garbern, J.Y., Simsek-Kiper, P.O., Ohashi, H., Robey, P.G., Boyde, A., Matsumoto, N., Miyake, N., Spranger, J., Schiffmann, R., Vanderver, A., Nishimura, G., Passos-Bueno, M.R.D.S., Simons, C., Ishikawa, K., Ikegawa, S., 2019. Bi-allelic CSF1R Mutations Cause Skeletal Dysplasia of Dysosteosclerosis-Pyle Disease Spectrum and Degenerative Encephalopathy with Brain Malformation. Am. J. Hum. Genet. 104, 925–935. https://doi.org/10.1016/j.ajhg.2019.03.004.

Haenseler, W., Sansom, S.N., Buchrieser, J., Newey, S.E., Moore, C.S., Nicholls, F.J., Chintawar, S., Schnell, C., Antel, J.P., Allen, N.D., Cader, M.Z., Wade-Martins, R., James, W.S., Cowley, S.A., 2017a. A Highly Efficient Human Pluripotent Stem Cell Microglia Model Displays a Neuronal-Co-culture-Specific Expression Profile and Inflammatory Response. Stem Cell Rep. 8, 1727–1742. https://doi.org/10.1016/j.stemcr.2017.05.017.

Haenseler, W., Zambon, F., Lee, H., Vowles, J., Rinaldi, F., Duggal, G., Houlden, H., Gwinn, K., Wray, S., Luk, K.C., Wade-Martins, R., James, W.S., Cowley, S.A., 2017b. Excess α-synuclein compromises phagocytosis in iPSC-derived macrophages. Sci. Rep. 7, 9003. https://doi.org/10.1038/s41598-017-09362-3.

Hagemeyer, N., Hanft, K.-M., Akriditou, M.-A., Unger, N., Park, E.S., Stanley, E.R., Staszewski, O., Dimou, L., Prinz, M., 2017. Microglia contribute to normal myelinogenesis and to oligodendrocyte progenitor maintenance during adulthood. Acta Neuropathol. 134, 441–458. https://doi.org/10.1007/s00401-017-1747-1.

Hagemeyer, N., Kierdorf, K., Frenzel, K., Xue, J., Ringelhan, M., Abdullah, Z., Godin, I., Wieghofer, P., Costa Jordão, M.J., Ulas, T., Yorgancioglu, G., Rosenbauer, F., Knolle, P.A., Heikenwalder, M., Schultze, J.L., Prinz, M., 2016. Transcriptome-based profiling of yolk sac-derived macrophages reveals a role for Irf8 in macrophage maturation. EMBO J. 35, 1730–1744. https://doi.org/10.15252/embj.201693801.

Haimon, Z., Volaski, A., Orthgiess, J., Boura-Halfon, S., Varol, D., Shemer, A., Yona, S., Zuckerman, B., David, E., Chappell-Maor, L., Bechmann, I., Gericke, M., Ulitsky, I., Jung, S., 2018. Re-evaluating microglia expression profiles using RiboTag and cell isolation strategies. Nat. Immunol. 19, 636–644. https://doi.org/10.1038/s41590-018-0110-6.

Hasselmann, J., Blurton-Jones, M., 2020. Human iPSC-derived microglia: A growing toolset to study the brain's innate immune cells. Glia 68, 721–739. https://doi.org/10.1002/glia.23781.

Hasselmann, J., Coburn, M.A., England, W., Figueroa Velez, D.X., Kiani Shabestari, S., Tu, C.H., McQuade, A., Kolahdouzan, M., Echeverria, K., Claes, C., Nakayama, T., Azevedo, R., Coufal, N.G., Han, C.Z., Cummings, B.J., Davtyan, H., Glass, C.K., Healy, L.M., Gandhi, S.P., Spitale, R.C., Blurton-Jones, M., 2019. Development of a chimeric model to study and manipulate human microglia in vivo. Neuron 103, 1016–1033.e10. https://doi.org/10.1016/j.neuron.2019.07.002.

Hayakawa, T., Angata, T., Lewis, A.L., Mikkelsen, T.S., Varki, N.M., Varki, A., 2005. A human-specific gene in microglia. Science 309, 1693. https://doi.org/10.1126/science.1114321.

Hickman, S.E., El Khoury, J., 2019. Analysis of the microglial sensome. Methods Mol. Biol. 2034, 305–323. https://doi.org/10.1007/978-1-4939-9658-2_23.

Holguin, A., Frank, M.G., Biedenkapp, J.C., Nelson, K., Lippert, D., Watkins, L.R., Rudy, J.W., Maier, S.F., 2007. Characterization of the temporo-spatial effects of chronic bilateral intrahippocampal cannulae on interleukin-1beta. J. Neurosci. Methods 161, 265–272. https://doi.org/10.1016/j.jneumeth.2006.11.014.

Johnson, B.S., Mueller, L., Si, J., Collins, S.J., 2002. The cytokines IL-3 and GM-CSF regulate the transcriptional activity of retinoic acid receptors in different in vitro models of myeloid differentiation. Blood 99, 746–753. https://doi.org/10.1182/blood.v99.3.746.

Kang, S.S., Ebbert, M.T.W., Baker, K.E., Cook, C., Wang, X., Sens, J.P., Kocher, J.-P., Petrucelli, L., Fryer, J.D., 2018. Microglial translational profiling reveals a convergent APOE pathway from aging, amyloid, and tau. J. Exp. Med. 215, 2235–2245. https://doi.org/10.1084/jem.20180653.

Kierdorf, K., Erny, D., Goldmann, T., Sander, V., Schulz, C., Perdiguero, E.G., Wieghofer, P., Heinrich, A., Riemke, P., Hölscher, C., Müller, D.N., Luckow, B., Brocker, T., Debowski, K., Fritz, G., Opdenakker, G., Diefenbach, A., Biber, K., Heikenwalder, M., Geissmann, F., Rosenbauer, F., Prinz, M., 2013. Microglia emerge from erythromyeloid precursors via Pu.1- and Irf8-dependent pathways. Nat. Neurosci. 16, 273–280. https://doi.org/10.1038/nn.3318.

Kim, K., Doi, A., Wen, B., Ng, K., Zhao, R., Cahan, P., Kim, J., Aryee, M.J., Ji, H., Ehrlich, L.I.R., Yabuuchi, A., Takeuchi, A., Cunniff, K.C., Hongguang, H., McKinney-Freeman, S., Naveiras, O., Yoon, T.J., Irizarry, R.A., Jung, N., Seita, J., Hanna, J., Murakami, P., Jaenisch, R., Weissleder, R., Orkin, S.H., Weissman, I.L., Feinberg, A.P., Daley, G.Q., 2010. Epigenetic memory in induced pluripotent stem cells. Nature 467, 285–290. https://doi.org/10.1038/nature09342.

Knuesel, I., Chicha, L., Britschgi, M., Schobel, S.A., Bodmer, M., Hellings, J.A., Toovey, S., Prinssen, E.P., 2014. Maternal immune activation and abnormal brain development across CNS disorders. Nat. Rev. Neurol. 10, 643–660. https://doi.org/10.1038/nrneurol.2014.187.

Konttinen, H., Cabral-da-Silva, M.E.C., Ohtonen, S., Wojciechowski, S., Shakirzyanova, A., Caligola, S., Giugno, R., Ishchenko, Y., Hernández, D., Fazaludeen, M.F., Eamen, S., Budia, M.G., Fagerlund, I., Scoyni, F., Korhonen, P., Huber, N., Haapasalo, A., Hewitt, A.W., Vickers, J., Smith, G.C., Oksanen, M., Graff, C., Kanninen, K.M., Lehtonen, S., Propson, N., Schwartz, M.P., Pébay, A., Koistinaho, J., Ooi, L., Malm, T., 2019. PSEN1ΔE9, APPswe, and APOE4 Confer Disparate Phenotypes in Human iPSC-Derived Microglia. Stem Cell Rep. 13, 669–683. https://doi.org/10.1016/j.stemcr.2019.08.004.

Leung, A., Ciau-Uitz, A., Pinheiro, P., Monteiro, R., Zuo, J., Vyas, P., Patient, R., Porcher, C., 2013. Uncoupling VEGFA functions in arteriogenesis and hematopoietic stem cell specification. Dev. Cell 24, 144–158. https://doi.org/10.1016/j.devcel.2012.12.004.

Liao, Y., Smyth, G.K., Shi, W., 2014. featureCounts: an efficient general purpose program for assigning sequence reads to genomic features. Bioinformatics 30, 923–930. https://doi.org/10.1093/bioinformatics/btt656.

Lin, Y.-T., Seo, J., Gao, F., Feldman, H.M., Wen, H.-L., Penney, J., Cam, H.P., Gjoneska, E., Raja, W.K., Cheng, J., Rueda, R., Kritskiy, O., Abdurrob, F., Peng, Z., Milo, B., Yu, C.J., Elmsaouri, S., Dey, D., Ko, T., Yankner, B.A., Tsai, L.-H., 2018. APOE4 Causes Widespread Molecular and Cellular Alterations Associated with Alzheimer's Disease Phenotypes in Human iPSC-Derived Brain Cell Types. Neuron 98, 1294. https://doi.org/10.1016/j.neuron.2018.06.011.

Livesey, M.R., Magnani, D., Cleary, E.M., Vasistha, N.A., James, O.T., Selvaraj, B.T., Burr, K., Story, D., Shaw, C.E., Kind, P.C., Hardingham, G.E., Wyllie, D.J.A., Chandran, S., 2016. Maturation and electrophysiological properties of human pluripotent stem cell-derived oligodendrocytes. Stem Cells 34, 1040–1053. https://doi.org/10.1002/stem.2273.

Lloyd, A.F., Davies, C.L., Holloway, R.K., Labrak, Y., Ireland, G., Carradori, D., Dillenburg, A., Borger, E., Soong, D., Richardson, J.C., Kuhlmann, T., Williams, A., Pollard, J.W., des Rieux, A., Priller, J., Miron, V.E., 2019. Central nervous system regeneration is driven by microglia necroptosis and repopulation. Nat. Neurosci. 22, 1046–1052. https://doi.org/10.1038/s41593-019-0418-z.

Love, M.I., Huber, W., Anders, S., 2014. Moderated estimation of fold change and dispersion for RNA-seq data with DESeq2. Genome Biol. 15, 550. https://doi.org/10.1186/s13059-014-0550-8.

Maechler, M., Rousseeuw, P., Struyf, A., Hubert, M., 2005. Cluster analysis basics and extensions. R package version 1 (12), 1.

Malavasi, E.L.V., Economides, K.D., Grünewald, E., Makedonopoulou, P., Gautier, P., Mackie, S., Murphy, L.C., Murdoch, H., Crummie, D., Ogawa, F., McCartney, D.L., O'Sullivan, S.T., Burr, K., Torrance, H.S., Phillips, J., Bonneau, M., Anderson, S.M., Perry, P., Pearson, M., Constantinides, C., Davidson-Smith, H., Kabiri, M., Duff, B., Johnstone, M., Polites, H.G., Lawrie, S.M., Blackwood, D.H., Semple, C.A., Evans, K.L., Didier, M., Chandran, S., McIntosh, A.M., Price, D.J., Houslay, M.D., Porteous, D.J., Millar, J.K., 2018. DISC1 regulates N-methyl-D-aspartate receptor dynamics: abnormalities induced by a Disc1 mutation modelling a translocation linked to major mental illness. Transl. Psychiatry 8, 184. https://doi.org/10.1038/s41398-018-0228-1.

Marín-Teva, J.L., Dusart, I., Colin, C., Gervais, A., van Rooijen, N., Mallat, M., 2004. Microglia promote the death of developing Purkinje cells. Neuron 41, 535–547. https://doi.org/10.1016/s0896-6273(04)00069-8.

Masuda, T., Sankowski, R., Staszewski, O., Böttcher, C., Amann, L., Sagar, Scheiwe, C.,

Nessler, S., Kunz, P., van Loo, G., Coenen, V.A., Reinacher, P.C., Michel, A., Sure, U., Gold, R., Grün, D., Priller, J., Stadelmann, C., Prinz, M., 2019. Spatial and temporal heterogeneity of mouse and human microglia at single-cell resolution. Nature 566, 388–392. https://doi.org/10.1038/s41586-019-0924-x.

Matcovitch-Natan, O., Winter, D.R., Giladi, A., Vargas Aguilar, S., Spinrad, A., Sarrazin, S., Ben-Yehuda, H., David, E., Zelada González, F., Perrin, P., Keren-Shaul, H., Gury, M., Lara-Astaiso, D., Thaiss, C.A., Cohen, M., Bahar Halpern, K., Baruch, K., Deczkowska, A., Lorenzo-Vivas, E., Itzkovitz, S., Elinav, E., Sieweke, M.H., Schwartz, M., Amit, I., 2016. Microglia development follows a stepwise program to regulate brain homeostasis. Science 353, aad8670. https://doi.org/10.1126/science.aad8670.

McQuade, A., Coburn, M., Tu, C.H., Hasselmann, J., Davtyan, H., Blurton-Jones, M., 2018. Development and validation of a simplified method to generate human microglia from pluripotent stem cells. Mol. Neurodegener. 13, 67. https://doi.org/10.1186/s13024-018-0297-x.

Melief, J., Sneeboer, M.A.M., Litjens, M., Ormel, P.R., Palmen, S.J.M.C., Huitinga, I., Kahn, R.S., Hol, E.M., de Witte, L.D., 2016. Characterizing primary human microglia: A comparative study with myeloid subsets and culture models. Glia 64, 1857–1868. https://doi.org/10.1002/glia.23023.

Muffat, J., Li, Y., Yuan, B., Mitalipova, M., Omer, A., Corcoran, S., Bakiasi, G., Tsai, L.-H., Aubourg, P., Ransohoff, R.M., Jaenisch, R., 2016. Efficient derivation of microglia-like cells from human pluripotent stem cells. Nat. Med. 22, 1358–1367. https://doi.org/10.1038/nm.4189.

Nimmerjahn, A., Kirchhoff, F., Helmchen, F., 2005. Resting microglial cells are highly dynamic surveillants of brain parenchyma in vivo. Science 308, 1314–1318. https://doi.org/10.1126/science.1110647.

Nugent, A.A., Lin, K., van Lengerich, B., Lianoglou, S., Przybyla, L., Davis, S.S., Llapashtica, C., Wang, J., Kim, D.J., Xia, D., Lucas, A., Baskaran, S., Haddick, P.C.G., Lenser, M., Earr, T.K., Shi, J., Dugas, J.C., Andreone, B.J., Logan, T., Solanoy, H.O., Chen, H., Srivastava, A., Poda, S.B., Sanchez, P.E., Watts, R.J., Sandmann, T., Astarita, G., Lewcock, J.W., Monroe, K.M., Di Paolo, G., 2020. TREM2 Regulates Microglial Cholesterol Metabolism upon Chronic Phagocytic Challenge. Neuron 105, 837–854.e9. https://doi.org/10.1016/j.neuron.2019.12.007.

Oosterhof, N., Chang, I.J., Karimiani, E.G., Kuil, L.E., Jensen, D.M., Daza, R., Young, E., Astle, L., van der Linde, H.C., Shivaram, G.M., Demmers, J., Latimer, C.S., Keene, C.D., Loter, E., Maroofian, R., van Ham, T.J., Hevner, R.F., Bennett, J.T., 2019. Homozygous Mutations in CSF1R Cause a Pediatric-Onset Leukoencephalopathy and Can Result in Congenital Absence of Microglia. Am. J. Hum. Genet. 104, 936–947. https://doi.org/10.1016/j.ajhg.2019.03.010.

Ormel, P.R., Vieira de Sá, R., van Bodegraven, E.J., Karst, H., Harschnitz, O., Sneeboer, M.A.M., Johansen, L.E., van Dijk, R.E., Scheefhals, N., Berdenis van Berlekom, A., Ribes Martínez, E., Kling, S., MacGillavry, H.D., van den Berg, L.H., Kahn, R.S., Hol, E.M., de Witte, L.D., Pasterkamp, R.J., 2018. Microglia innately develop within cerebral organoids. Nat. Commun. 9, 4167. https://doi.org/10.1038/s41467-018-06684-2.

Pandya, H., Shen, M.J., Ichikawa, D.M., Sedlock, A.B., Choi, Y., Johnson, K.R., Kim, G., Brown, M.A., Elkahloun, A.G., Maric, D., Sweeney, C.L., Gossa, S., Malech, H.L., McGavern, D.B., Park, J.K., 2017. Differentiation of human and murine induced pluripotent stem cells to microglia-like cells. Nat. Neurosci. 20, 753–759. https://doi.org/10.1038/nn.4534.

Park, I.-H., Zhao, R., West, J.A., Yabuuchi, A., Huo, H., Ince, T.A., Lerou, P.H., Lensch, M.W., Daley, G.Q., 2008. Reprogramming of human somatic cells to pluripotency with defined factors. Nature 451, 141–146. https://doi.org/10.1038/nature06534.

Piers, T.M., Cosker, K., Mallach, A., Johnson, G.T., Guerreiro, R., Hardy, J., Pocock, J.M., 2020. A locked immunometabolic switch underlies TREM2 R47H loss of function in human iPSC-derived microglia. FASEB J. 34, 2436–2450. https://doi.org/10.1096/fj.201902447R.

Prinz, M., Priller, J., 2014. Microglia and brain macrophages in the molecular age: from origin to neuropsychiatric disease. Nat. Rev. Neurosci. 15, 300–312. https://doi.org/10.1038/nrn3722.

Risso, D., Ngai, J., Speed, T.P., Dudoit, S., 2014. Normalization of RNA-seq data using factor analysis of control genes or samples. Nat. Biotechnol. 32, 896–902. https://doi.org/10.1038/nbt.2931.

Rowe, R.G., Daley, G.Q., 2019. Induced pluripotent stem cells in disease modelling and drug discovery. Nat. Rev. Genet. 20, 377–388. https://doi.org/10.1038/s41576-019-0100-z.

Schafer, D.P., Lehrman, E.K., Kautzman, A.G., Koyama, R., Mardinly, A.R., Yamasaki, R., Ransohoff, R.M., Greenberg, M.E., Barres, B.A., Stevens, B., 2012. Microglia sculpt postnatal neural circuits in an activity and complement-dependent manner. Neuron 74, 691–705. https://doi.org/10.1016/j.neuron.2012.03.026.

Schulz, C., Gomez Perdiguero, E., Chorro, L., Szabo-Rogers, H., Cagnard, N., Kierdorf, K., Prinz, M., Wu, B., Jacobsen, S.E.W., Pollard, J.W., Frampton, J., Liu, K.J., Geissmann, F., 2012. A lineage of myeloid cells independent of Myb and hematopoietic stem cells. Science 336, 86–90. https://doi.org/10.1126/science.1219179.

Sellgren, C.M., Gracias, J., Watmuff, B., Biag, J.D., Thanos, J.M., Whittredge, P.B., Fu, T., Worringer, K., Brown, H.E., Wang, J., Kaykas, A., Karmacharya, R., Goold, C.P., Sheridan, S.D., Perlis, R.H., 2019. Increased synapse elimination by microglia in schizophrenia patient-derived models of synaptic pruning. Nat. Neurosci. 22, 374–385. https://doi.org/10.1038/s41593-018-0334-7.

Sierra, A., Encinas, J.M., Deudero, J.J.P., Chancey, J.H., Enikolopov, G., Overstreet-Wadiche, L.S., Tsirka, S.E., Maletic-Savatic, M., 2010. Microglia shape adult hippocampal neurogenesis through apoptosis-coupled phagocytosis. Cell Stem Cell 7, 483–495. https://doi.org/10.1016/j.stem.2010.08.014.

Slukvin, I.I., 2013. Hematopoietic specification from human pluripotent stem cells: current advances and challenges toward de novo generation of hematopoietic stem cells. Blood 122, 4035–4046. https://doi.org/10.1182/blood-2013-07-474825.

Squarzoni, P., Oller, G., Hoeffel, G., Pont-Lezica, L., Rostaing, P., Low, D., Bessis, A., Ginhoux, F., Garel, S., 2014. Microglia modulate wiring of the embryonic forebrain. Cell Rep. 8, 1271–1279. https://doi.org/10.1016/j.celrep.2014.07.042.

Stephens, M., 2017. False discovery rates: a new deal. Biostatistics 18, 275–294. https://doi.org/10.1093/biostatistics/kxw041.

Svoboda, D.S., Barrasa, M.I., Shu, J., Rietjens, R., Zhang, S., Mitalipova, M., Berube, P., Fu, D., Shultz, L.D., Bell, G.W., Jaenisch, R., 2019. Human iPSC-derived microglia assume a primary microglia-like state after transplantation into the neonatal mouse brain. Proc. Natl. Acad. Sci. USA 116, 25293–25303. https://doi.org/10.1073/pnas.1913541116.

Szklarczyk, D., Gable, A.L., Lyon, D., Junge, A., Wyder, S., Huerta-Cepas, J., Simonovic, M., Doncheva, N.T., Morris, J.H., Bork, P., Jensen, L.J., von Mering, C., 2019. STRING v11: protein-protein association networks with increased coverage, supporting functional discovery in genome-wide experimental datasets. Nucleic Acids Res. 47, D607–D613. https://doi.org/10.1093/nar/gky1131.

Takahashi, K., Yamanaka, S., 2006. Induction of pluripotent stem cells from mouse embryonic and adult fibroblast cultures by defined factors. Cell 126, 663–676. https://doi.org/10.1016/j.cell.2006.07.024.

Telezhkin, V., Straccia, M., Yarova, P., Pardo, M., Yung, S., Vinh, N.-N., Hancock, J.M., Barriga, G.G.-D., Brown, D.A., Rosser, A.E., Brown, J.T., Canals, J.M., Randall, A.D., Allen, N.D., Kemp, P.J., 2018. Kv7 channels are upregulated during striatal neuron development and promote maturation of human iPSC-derived neurons. Pflugers Arch. 470, 1359–1376. https://doi.org/10.1007/s00424-018-2155-7.

Tremblay, M.-È., Lowery, R.L., Majewska, A.K., 2010. Microglial interactions with synapses are modulated by visual experience. PLoS Biol. 8, e1000527. https://doi.org/10.1371/journal.pbio.1000527.

Ueno, M., Fujita, Y., Tanaka, T., Nakamura, Y., Kikuta, J., Ishii, M., Yamashita, T., 2013. Layer V cortical neurons require microglial support for survival during postnatal development. Nat. Neurosci. 16, 543–551. https://doi.org/10.1038/nn.3358.

van Wilgenburg, B., Browne, C., Vowles, J., Cowley, S.A., 2013. Efficient, long term production of monocyte-derived macrophages from human pluripotent stem cells under partly-defined and fully-defined conditions. PLoS One 8, e71098. https://doi.org/10.1371/journal.pone.0071098.

Visentin, S., Agresti, C., Patrizio, M., Levi, G., 1995. Ion channels in rat microglia and their different sensitivity to lipopolysaccharide and interferon-gamma. J. Neurosci. Res. 42, 439–451. https://doi.org/10.1002/jnr.490420402.

Wickham, H., 2016. ggplot2: elegant graphics for data analysis.

Yoshihara, M., Hayashizaki, Y., Murakawa, Y., 2017. Genomic Instability of iPSCs: Challenges Towards Their Clinical Applications. Stem Cell Rev and Rep 13, 7–16. https://doi.org/10.1007/s12015-016-9680-6.

Zerbino, D.R., Achuthan, P., Akanni, W., Amode, M.R., Barrell, D., Bhai, J., Billis, K., Cummins, C., Gall, A., Girón, C.G., Gil, L., Gordon, L., Haggerty, L., Haskell, E., Hourlier, T., Izuogu, O.G., Janacek, S.H., Juettemann, T., To, J.K., Laird, M.R., Lavidas, I., Liu, Z., Loveland, J.E., Maurel, T., McLaren, W., Moore, B., Mudge, J., Murphy, D.N., Newman, V., Nuhn, M., Ogeh, D., Ong, C.K., Parker, A., Patricio, M., Riat, H.S., Schuilenburg, H., Sheppard, D., Sparrow, H., Taylor, K., Thormann, A., Vullo, A., Walts, B., Zadissa, A., Frankish, A., Hunt, S.E., Kostadima, M., Langridge, N., Martin, F.J., Muffato, M., Perry, E., Ruffier, M., Staines, D.M., Trevanion, S.J., Aken, B.L., Cunningham, F., Yates, A., Flicek, P., 2018. Ensembl 2018. Nucleic Acids Res. 46, D754–D761. https://doi.org/10.1093/nar/gkx1098.